A Multiple Extended Object Tracker with the Gaussian Process Model Utilizing Negative Information

MARTIN BAERVELDT
MICHAEL ERNESTO LÓPEZ
EDMUND FØRLAND BREKKE

In multiple extended object tracking, the Poisson multi-Bernoulli mixture (PMBM) tracker is considered state-of-the-art. Originally, it was presented with the gamma Gaussian inverse Wishart (GGIW) target model, which is a random matrix model. When tracking larger objects using a light detection and ranging (LiDAR) sensor, measurements are generated by the contour rather than the whole target surface, and it is beneficial to model this with the target model. A target model that has this capability is the Gaussian process (GP) extent model. This paper presents a PMBM tracker using this target model. We also discuss considerations related to the use of the GP model in the PMBM framework. Secondly, we present improvements in the target model that increase the robustness of the model by dealing with the inherent non-linearities using the Gauss–Newton method. Furthermore, we incorporate an improvement to the tracker that utilizes the concept of negative information to generate virtual measurements that are then used in the Gauss–Newton optimization. In relation to this, we also present an occlusion model that utilizes the same negative information model to ensure that the state estimate is consistent in the presence of occluding targets. The presented methods are compared to the GGIW-PMBM tracker on simulated and real LiDAR data gathered from maritime vessels. The results show that the GP model outperforms the GGIW model by providing a better estimate of the extent and more accurate tracking, as measured by the GOSPA metric. Utilizing negative information for state estimation and occlusion modeling further improves the state estimate and tracking performance.

Manuscript received March 25, 2024; revised July 8, 2024; released for publication January 10, 2025

Refereeing of this contribution was handled by Florian Meyer.

The work was supported by the European Union's Horizon 2020 research and innovation programme under the Marie Skłodowska-Curie grant agreement No. 955.768 (MSCA-ETN AUTOBarge). This publication reflects only the authors' view, exempting the European Union from any liability. Project website: http://etn-autobarge.eu/. This work was supported in part by the Research Council of Norway through Projects 295033 and 309230.

The authors are with the Department of Engineering Cybernetics, Norwegian University of Science and Technology, 7034 Trondheim, Norway (e-mail: martin.baerveldt@ntnu.no; ernesto.lopez@ntnu.no; edmund.brekke@ntnu.no).

1557-6418/2024/$17.00

I. INTRODUCTION

Target tracking, the issue of estimating the kinematic state of one or several objects, has long used the point approximation when parsing sensor data. With the advent of high-resolution sensors, it is now common that a measurement source gives rise to multiple measurements. This has given rise to extended object tracking models, which enable the modeling of a target's extent in addition to its kinematic properties by inferring information from the spatial distribution of these measurements [1]. Initial approaches assumed that the spatial distribution of the measurements could be modeled by a Gaussian distribution around the center of the target extent. This results in an estimated ellipsoidal extent [2]. This is known as the random matrix model. A version of this model, the gamma Gaussian inverse Wishart (GGIW) model, was used to demonstrate an extended object Poisson multi-Bernoulli mixture (PMBM) filter [3] based on the original PMBM filter [4]. This filter has also been used with a set of trajectory framework [5]. Work has also been conducted to investigate improvements with regard to data association [6] and reducing complexity by approximating the PMBM posterior as a PMB [7]. In [8], a factor graph representation of the PMBM posterior was used to present a PMB filter using the particle belief propagation method presented in [9]. However, the random matrix model is not the only target model for extended objects. Another method, the random hypersurface model, models the extent using star-convex shapes and represents the shape using a parametrization of the contour [10]. This enables the modeling of more complex shapes. It also allows an easier way to model measurements that originate from the contour, such as measurements generated by an LiDAR sensor. The most promising and investigated of these models uses Gaussian processes (GP) to estimate the extent [11]. This model has been further improved with different estimation methods [12], [13] and augmented with the use of virtual measurements that use negative information [14].

The GP model has also been used to implement multi-object tracking filters, such as the δ-GLMB filter [15] and the probability hypothesis density (PHD) filter [16]. In previous work comparing different filter structures, it has been shown that the PMBM has a more efficient structure and it can initialize a track faster with its Poisson birth model as compared to Bernoulli birth models [17].

A key challenge to consider for multiple extended object tracking is occlusion, since this will cause objects to not generate measurements. Previous methods have looked at the specific target model and calculated a non-constant probability of detection [18], [19] based on the state of other targets using the GGIW model; this has also been done in the context of the extended object PMBM filter [3]. Another approach was presented in [20], which calculates an occlusion likelihood based on random variables inferred from the current set of targets. This occlusion likelihood is represented by a Gaussian mixture, which can be used to update the state of undetected objects, infer the existence of objects, and inform data association.

In this paper, we aim to present an extended object PMBM tracker using the GP target model with the applicable prediction and update formulas. We also provide an example of a Poisson birth density for the GP target model. Furthermore, we introduce an improvement to dealing with the nonlinearity of the measurement model for the GP target model. In addition, we present a method to incorporate negative information into the estimate of object states for this model by the use of virtual measurements, similar to the method in [14]. To ensure that this can be utilized in a multi-object context, we also utilize these virtual measurements to model target occlusion. Finally, we show the application of the developed tracker on LiDAR data gathered by tracking smaller maritime vessels. This article is an extension of [21] with the additional inclusion of the method of using negative information for state estimation and occlusion handling, as well as a refined criterion for initialization for the Gauss–Newton (GN) optimization. It also includes a more complex simulation scenario and a more detailed exposition of the method. The article is organized as follows: In Section II, we introduce the relevant theory and previous work, and in Section III, we present the improvement to the GP target model, along with the incorporation of negative information into the state estimation. In Section IV, we present the applicable prediction and update formulas for a PMBM filter utilizing the GP target model, the specific approximations that are used in this paper, as well as the utilization of negative information to model occlusion. In Section V, we present the simulation study, and in Section VI, the results on the real maritime data are presented.

II. BACKGROUND

In this section, we present a summary of the method of extent estimation using GP presented in [11]. Then we outline the theory related to the extended object PMBM filter, which was presented in [3].

A. Notation

In the following, we present the most significant variables as well as the notation used in this work.

NOMENCLATURE

$(\cdot)^*$	Quantities related to the virtual measurements.
$(\cdot)^b$	Quantities related to the birth process.
$(\cdot)^f$	Quantities related to the radial function f.
$(\cdot)^u$	Quantities related to unknown targets.
$(\cdot)_n^u/(\cdot)_{u_n}$	Quantities related to nth component of the PPP intensity of unknown targets.
$(\cdot)^{j,i}$	Quantities related to the ith Bernoulli in the jth multi-Bernoulli in an MBM.
$(\cdot)_k$	Quantity at time step k.
α	Shape parameter of gamma distribution.
β	Inverse scale parameter of gamma distribution.
η_f	Forgetting factor for extent prediction.
η_v	Occlusion correction factor for gamma distribution.
η_γ	Forgetting factor for gamma prediction.
$\hat{(\cdot)}$	Estimation of a random variable.
$\kappa_{min/max}$	The minimum and maximum angle occupied by an extended object.
λ_c	Clutter rate.
λ_m	Measurement rate.
$\mathbb{I}$	Set of targets in a multi-Bernoulli.
$\mathbb{I}_O^{j,i}$	Set of occluding targets for target i in the jth MB.
$\mathbb{I}_{pO}^{j,i}$	Set of partially occluding targets for target i in the jth MB.
$\mathbb{J}$	Set of components in an MBM.
$\mathbf{F}$	Process model transition matrix.
$\mathbf{H}$	Measurement matrix.
$\mathbf{h}(\mathbf{x})$	Vector of predicted measurements for a target.
$\mathbf{P}$	State covariance matrix.
$\mathbf{Q}$	Process noise covariance matrix.
$\mathbf{R}$	Measurement noise covariance matrix.
$\mathbf{x}$	State space vector of a target.
$\mathbf{x}^c$	Position of target centroid.
$\mathbf{z}_k$	Vector of measurements for one scan at timestep k.
ϕ	Heading of a target.
$\sigma_{(\cdot)}$	Standard deviation of a quantity.
θ	Angle used in the radial function f.
D	A PPP intensity function.
f	Probability density function.
$f(\theta)$	Radial function which is estimated by a GP.
$k(\theta, \theta')$	Covariance function for a GP.
L_C^j	Likelihood of measurement cell assignment.
l_C	Predictive likelihood of a measurement set being assigned to an estimated target.
P_D	Probability of detection.
P_G	Gating probability.
P_O	Probability of occlusion.
P_S	Probability of survival.
P_{pO}	Probability of partial occlusion.
Q_D	Probability of missed detection.
r	Existence probability.
T	Sampling time.
v^i	Visibility ratio of object i.
w^j	Weight of the jth multi-Bernoulli in an MBM.
w_e	Window length of gamma prediction.
z^l	The lth measurement in a set.
$\theta^{(G)}$	θ defined in the global frame.
$\theta^{(L)}$	θ defined in the local target frame.

B. Gaussian Process

A GP can be considered a distribution over functions [22]. It is completely specified by its mean function $m(\gamma)$ and covariance function $k(\gamma, \gamma')$. Using GPs to estimate a radial function means that we can write

$$f(\theta) \sim \mathcal{GP}(m(\theta), k(\theta, \theta')), \tag{1}$$

where $f(\theta)$ defines the radius at angle θ. We want to estimate the values of this function using measurements of only some of its values. This is a method known as GP regression. We define a vector of N different points known as test points $\Theta^f = [\theta_1^f \quad ... \quad \theta_N^f]$. Further, we define a measurement model as

$$z_k = f(\theta_k) + \eta_k, \quad \eta_k \sim \mathcal{N}(0, \mathbf{R}), \tag{2}$$

where z_k is a measurement of the unknown function, θ_k is the training input, which is the point at which the measurement is taken, and η_k is the measurement noise. If we have m measurements of the function, we define $\mathbf{z} = [z^1 \quad ... \quad z^m]$ and their corresponding input values $\Theta = [\theta_1 \quad ... \quad \theta_m]$ to learn the function values for Θ^f. In the original paper [11], it is shown that the state $\mathbf{x}^f = \left[f(\theta_1^f) \quad ... \quad f(\theta_N^f)\right]^\mathsf{T}$, which defines the extent, can be recursively estimated using the following state space model:

$$\begin{aligned} \mathbf{x}_{k+1}^f &= \mathbf{F}^f \mathbf{x}_k^f + \mathbf{w}_k, \quad \mathbf{w}_k \sim \mathcal{N}(0, \mathbf{Q}^f) \\ z_k &= \mathbf{H}^f(\theta_k)\mathbf{x}_k^f + \epsilon_k^f, \quad \epsilon_k^f \sim \mathcal{N}(0, \mathbf{R}^f). \end{aligned} \tag{3}$$

The measurement model is in turn given by the following matrices:

$$\begin{aligned} \mathbf{H}^f(\theta_k) &= \mathbf{K}(\theta_k, \Theta^f)\left[\mathbf{K}(\Theta^f, \Theta^f)\right]^{-1} \\ \mathbf{R}^f(\theta_k) &= k(\theta_k, \theta_k) + \mathbf{R} - \mathbf{H}^f(\theta_k)\mathbf{K}(\Theta^f, \theta_k), \end{aligned} \tag{4}$$

where $\mathbf{K}$ in turn is defined as a covariance matrix where the elements are made up of the elementwise evaluation of the covariance function $k(\theta, \theta')$. The process model is defined by

$$\mathbf{F}^f = e^{-\eta_f T}\mathbf{I}, \quad \mathbf{Q}^f = \left(1 - e^{-2\eta_f T}\right)\mathbf{K}(\Theta^f, \Theta^f), \tag{5}$$

where T is the sampling time. The parameter for this model is a forgetting factor η_f.

1) Covariance Functions: As can be inferred from the equations above, the covariance function is the component that defines the GP and any prior information about the shapes. Therefore, we want to encode the periodicity of $f(\theta)$ in the covariance function. Such a function was presented in the original article as

$$k(\theta, \theta') = \sigma_f^2 e^{-\frac{1}{2l^2}\left(\sin^2\frac{|\theta-\theta'|}{2}\right)} + \sigma_r^2. \tag{6}$$

This function gives a high correlation for two function values $f(\theta)$ and $f(\theta')$ when their respective angles are closer and a lower correlation when they are further apart. σ_f, the signal variance, defines the magnitude of this correlation, and the length-scale l defines the distance on which it acts. σ_r is a constant bias term, which can be used to formulate the GP as a zero mean GP by stating $m(\theta) \sim \mathcal{N}(0, \sigma_r^2)$, integrating out $m(\theta)$, and adding it as a contribution to the covariance function.

It is also desirable to design a covariance function that encodes axial symmetry since, in many cases, targets are symmetric about the longitudinal axis. Since the longitudinal axis is defined at $\theta = 0$, this is equivalent to an even function. One such function can be built using the smallest signed angle function

$$ssa(\theta) := \pi - [(\pi - \theta)(\mathrm{mod}2\pi)], \tag{7}$$

i.e., $ssa(\theta)$ is the only angle in $(-\pi, \pi]$ such that $ssa(\theta) \equiv \theta$. The absolute value of this function is both 2π-periodic and even, which is equivalent to the radial curve of $f(\theta)$ being closed and symmetric about the longitudinal axis, as desired. We define the symmetric covariance function as

$$k(\theta, \theta') = \sigma_f^2 e^{-\frac{1}{2l^2}(|ssa(\theta)| - |ssa(\theta')|)^2} + \sigma_r^2 + \sigma_n^2 \delta(\theta, \theta'), \tag{8}$$

where σ_n is a noise term that models individual features of a specific point, such as a sharp corner, by adding a small term to each diagonal part of the constructed covariance matrix. This has the added benefit of regularizing the covariance matrix [23].

C. State Space Model for Extended Targets

To perform joint estimation of the extent and state of the target, an augmented state space vector is defined

$$\mathbf{x}_k = \left[\mathbf{x}_k^{c\,\mathsf{T}} \quad \phi_k \quad \left(\mathbf{x}_k^{*\mathsf{T}}\right) \quad \mathbf{x}_k^{f\,\mathsf{T}}\right]^\mathsf{T}, \tag{9}$$

where $\mathbf{x}_k^c$ is the position of the centroid of the target from which the extent is defined, ϕ is the heading of the target, and $\mathbf{x}_k^*$ are any additional kinematic states of the target. In the original paper, these are the velocity in each direction in 2D $\dot{\mathbf{x}}_k^c$, and the angular velocity $\dot{\phi}_k$. We use the same state space vector in this paper.

For this augmented state space vector, we define the following state space description:

$$\begin{aligned} \mathbf{x}_{k+1} &= \mathbf{F}\mathbf{x}_k + \mathbf{w}, \quad \mathbf{w} \sim \mathcal{N}(0, \mathbf{Q}) \\ \mathbf{z}_k &= \mathbf{h}_k(\mathbf{x}_k) + \boldsymbol{\eta}_k, \quad \boldsymbol{\eta}_k \sim \mathcal{N}(0, \mathbf{R}_k), \end{aligned} \tag{10}$$

where $\mathbf{z}_k, \mathbf{h}_k(\mathbf{x}_k)$, and $\mathbf{R}_k$ are all augmentations given by measurements of one scan of the target

$$\begin{aligned} \mathbf{z}_k &= \left[\mathbf{z}_k^{1\,\mathsf{T}}, \quad ..., \quad \mathbf{z}_k^{m\,\mathsf{T}}\right]^\mathsf{T} \\ \mathbf{R}_k &= \mathrm{diag}\left[\mathbf{R}_k^1, \quad ..., \quad \mathbf{R}_k^m\right] \\ \mathbf{h}_k(\mathbf{x}_k) &= \left[\mathbf{h}_k^1(\mathbf{x}_k)^\mathsf{T}, \quad ..., \quad \mathbf{h}_k^m(\mathbf{x}_k)^\mathsf{T}\right]^\mathsf{T}. \end{aligned} \tag{11}$$

To define the measurement equation $\mathbf{h}_k^l(\mathbf{x}_k)$ for a single measurement $\mathbf{z}_k^l$, we utilize the measurement equation defined by the random hypersurface model for a target contour parametrized by a function f.

$$\begin{aligned} \mathbf{z}_k^l &= \mathbf{x}_k^c + \mathbf{p}(\theta_k^l) f(\theta_k^l) + \boldsymbol{\eta}_k^l \\ \mathbf{p}(\theta_k^l) &= \begin{bmatrix} \cos\theta_k^l \\ \sin\theta_k^l \end{bmatrix}, \end{aligned} \tag{12}$$

where $\mathbf{z}_k^l$ is the measurement l at time k and θ_k^l is the corresponding angle of the origin of the measurement of the target contour. θ_k^l can be expressed both in a global

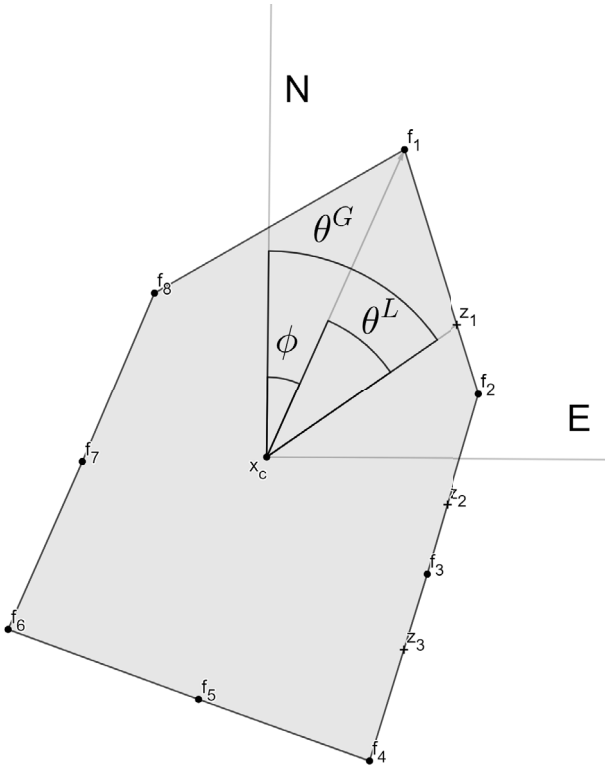

Figure 1. Visualization of the variables used in the measurement equation of the GP target model. The global frame is defined by N - North and E - East. The points marked with f_n correspond to the n-th element of $\mathbf{x}^f$, i.e., the test points, and the crosses marked with z_n represents measurements of the contour. The visualized θ^G and θ^L correspond to $\theta_k^{1\,(G)}(\mathbf{x}_k^c)$ and $\theta_k^{1\,(L)}(\mathbf{x}_k^c, \phi_k)$ respectively, i.e., they are defined for z_1.

frame $\theta_k^{l\,(G)}$ and the local target frame $\theta_k^{l\,(L)}$ as

$$\begin{aligned} \theta_k^{l\,(L)}(\mathbf{x}_k^c, \phi_k) &= \theta_k^{l\,(G)}(\mathbf{x}_k^c) - \phi_k \\ \theta_k^{l\,(G)}(\mathbf{x}_k^c) &= \angle\left(\mathbf{z}_{k,l} - \mathbf{x}_k^c\right). \end{aligned} \tag{13}$$

Inserting the expressions for GP regression (3) into the measurement equation (12), we attain

$$\begin{aligned} \mathbf{z}_k^l &= \mathbf{x}_k^c + \mathbf{p}_k^l(\theta_k^{l\,(G)}(\mathbf{x}_k^c))\mathbf{H}^f\left(\theta_k^{l\,(L)}(\mathbf{x}_k^c, \phi_k)\right)\mathbf{x}_k^f + \boldsymbol{\eta}_k^l \\ &= \mathbf{h}_k^l(\mathbf{x}_k) + \boldsymbol{\eta}_k^l, \qquad \boldsymbol{\eta}_k^l \sim \mathcal{N}(0, \mathbf{R}_k^l) \\ \mathbf{R}_k^l &= \mathbf{p}_k^l(\theta_k^{l\,(G)}(\mathbf{x}_k^c))\mathbf{R}^f\left(\theta_k^{l\,(L)}(\mathbf{x}_k^c, \phi_k)\right)\mathbf{p}_k^l(\theta_k^{l\,(G)}(\mathbf{x}_k^c))^\mathsf{T} + \mathbf{R}. \end{aligned} \tag{14}$$

This is a nonlinear measurement model and therefore needs to be estimated using a nonlinear filtering technique. It should be noted that this is an implicit equation due to the dependence of $\mathbf{z}_k^l$ contained in $\theta_k^{l\,(G)}(\mathbf{x}_k^c)$. See Fig. 1 for a graphical representation of the relationship between the variables used in the measurement equation.

For the motion model, the motion can be described with a linear state space model and this can be combined with the process model for the extent as

$$\mathbf{F} = \begin{bmatrix} \bar{\mathbf{F}} & 0 \\ 0 & \mathbf{F}^f \end{bmatrix}, \mathbf{Q} = \begin{bmatrix} \bar{\mathbf{Q}} & 0 \\ 0 & \mathbf{Q}^f \end{bmatrix}, \tag{15}$$

where $\mathbf{F}^f$ and $\mathbf{Q}^f$ are given by (5), and $\bar{\mathbf{F}}$ and $\bar{\mathbf{Q}}$ are given by the motion model used. For this work, we use the constant velocity model combined with a constant angular velocity. The model matrices are defined as

$$\begin{aligned} \bar{\mathbf{F}} &= \begin{bmatrix} 1 & T \\ 0 & 1 \end{bmatrix} \otimes \mathbf{I}_3, \\ \bar{\mathbf{Q}} &= \begin{bmatrix} \frac{T^3}{3} & \frac{T^2}{2} \\ \frac{T^2}{2} & T \end{bmatrix} \otimes \begin{bmatrix} \sigma_c^2 & 0 & 0 \\ 0 & \sigma_c^2 & 0 \\ 0 & 0 & \sigma_\phi^2 \end{bmatrix}, \end{aligned} \tag{16}$$

where σ_c is the standard deviation of the process noise for position and σ_ϕ is the standard deviation for the heading angle.

D. The PMBM Filter

To model the problem of tracking multiple targets, the PMBM filter utilizes random finite sets (RFS) to model both the unknown number of targets and the unknown number of measurements. The set of object states at time k is modeled as $X_k = \{x_k^1, \ldots, x_k^{n_k}\}$ and the measurements collected at time step k are defined as $Z_k = \{z_k^1, \ldots, z_k^{m_k}\}$ with z_k^l denoting a single measurement.

The PMBM conjugate prior is a combination of a Poisson point process (PPP) and a multi-Bernoulli mixture (MBM), where the PPP represents the targets that have not been detected $\mathbf{X}_k^u$ and the MBM represents the targets that have been detected $\mathbf{X}_k^d$. A PMBM density is fully parametrized by

$$D_k^u, \{w_k^j, \{r_k^{j,i}, (f_k^{j,i})\}_{i\in\mathbb{I}_{k|k'}}\}_{j\in\mathbb{J}_{k|k'}}, \tag{17}$$

where D_k^u is the intensity function of the PPP for the unknown targets. The Bernoulli modeling target i is represented by the probability density $f_k^{j,i}$, which represents both the kinematic state and the extent of the target, along with any additional information that can be inferred from it. A Bernoulli set also contains a parameter r that represents the existence probability of the target. The different components in the MBM are represented by an index $j \in \mathbb{J}$ and correspond to a data association hypothesis with the weight w^j representing the relative likelihood of each hypothesis. Additional assumptions are that new targets appear in the region according to a PPP with birth intensity function D_k^b, targets survive with probability P^S and evolve with a transition density $\mathbf{g}_{k|k-1}$. Clutter is modeled as a PPP with rate λ_c and a uniform spatial distribution. Each target is detected with a probability P^D and, if detected, generates measurements according to a PPP with rate $\lambda_m(\mathbf{x})$ and a spatial distribution $l(Z_C|\mathbf{x}_k)$, given by the chosen target model. Z_C is the subset of measurements assigned to a specific measurement cell C, and l_C is the likelihood of this assignment.

Recursions based on these assumptions are presented in the original paper on the PMBM filter for extended objects [3].

E. Estimating Measurement Rate

The Poisson rate $\lambda_m(\mathbf{x})$ models the cardinality of the measurement set, i.e., the expected number of measurements. The simplest assumption is a constant rate, but this is not in good agreement with the physical reality of many sensors, since the number of returns usually scales by distance. A more realistic approach was developed in [24] and has since been used as part of the GGIW target model in several works, such as [3], [25]. It has also been used in combination with the GP model [15]. It utilizes that a Poisson rate can be estimated using a gamma distribution because it is the conjugate prior to the Poisson distribution. A gamma distribution can be parametrized by parameters α and β, where α is the shape parameter and β is the inverse scale parameter, i.e., $\lambda_m \sim \mathcal{G}(\alpha, \beta)$. These can be updated using the following recursions:

$$\begin{aligned} \alpha_{k|k-1} &= \frac{\alpha_{k-1}}{\eta_\gamma}, \qquad \beta_{k|k-1} = \frac{\beta_{k-1}}{\eta_\gamma} \\ \alpha_k &= \alpha_{k|k-1} + |Z_C|, \qquad \beta_k = \beta_{k|k-1} + 1. \end{aligned} \tag{18}$$

The forgetting factor η_γ is defined as $\eta_\gamma = \frac{1}{1-\frac{1}{w_e}}$, which means that only information from the time steps within the window length w_e is trusted. By estimating these parameters for each target, we can determine a target-specific Poisson rate $\lambda_m(\mathbf{x})$ for each target.

III. IMPROVEMENTS TO THE GP TARGET MODEL

In this section, we present the suggested improvements to the GP target model by using the iterated extended Kalman filter to improve the linearization. We also present how negative information can be used in this framework.

A. Handling Nonlinearities in the Measurement Equation

Since the measurement equation (14) is nonlinear there arises a need to use nonlinear filtering to deal with this non-linearity and estimate $\mathbf{H}$. The original paper on the GP model applies the extended Kalman filter [11]. Subsequent work has been done to improve this method by dealing with the non-linearities differently or augmenting the approach [12]–[14]. In this work, we propose using the iterated extended Kalman filter (IEKF) to improve the linearization. It has been shown that applying the IEKF is equivalent to GN optimization of the maximum likelihood function defined as

$$q(\boldsymbol{\xi}) = \left(\begin{bmatrix} \mathbf{z}_k \\ \hat{\mathbf{x}} \end{bmatrix} - \begin{bmatrix} \mathbf{h}(\boldsymbol{\xi}) \\ \boldsymbol{\xi} \end{bmatrix} \right)^{\mathsf{T}} \begin{bmatrix} \mathbf{R} & 0 \\ 0 & \mathbf{P} \end{bmatrix}^{-1} \left(\begin{bmatrix} \mathbf{z}_k \\ \hat{\mathbf{x}} \end{bmatrix} - \begin{bmatrix} \mathbf{h}(\boldsymbol{\xi}) \\ \boldsymbol{\xi} \end{bmatrix} \right). \tag{19}$$

Here, $\mathbf{h}(\boldsymbol{\xi})$ and $\mathbf{z}_k$ are defined by (11) and (14). The IEKF is therefore a maximum a posteriori estimator of the state [26]. Equivalently, the IEKF will suffer from the same shortcomings as GN methods, in particular when there are several local optima or the initialization point is far away. In this specific case, $\mathbf{h}(\boldsymbol{\xi})$ is not globally convex and has several local optima.

To mitigate this, we suggest designing a set of heuristic constraints for the initial point of the optimization to ensure that it converges on the most relevant local optimum. In [14], the concept of negative information is used to augment the model. Inspired by this, we can define constraints for the centroid $\mathbf{x}^c$ for a given target. Consider a return from a laser- ranging sensor hitting an extended object. We can then state the following constraint for $\mathbf{x}^c := [x^p, y^p]$ given more than two measurements:

$$\begin{aligned} &\min(\angle \mathbf{z}_k) < \operatorname{atan2}(y^p, x^p) < \max(\angle \mathbf{z}_k) \\ &\min ||\mathbf{z}_k|| < \sqrt{(y^p)^2 + (x^p)^2}. \end{aligned} \tag{20}$$

Essentially, the center of the extended object's angle with regard to the sensor should be between the minimum and maximum angles, and it should be further away than the closest measurement return. We enforce this condition prior to optimization by first calculating the mean range and angle of the measurements generated by the contour

$$\begin{aligned} \theta^c &= \operatorname{mean}(\angle \mathbf{z}_k) \\ r^c &= \operatorname{mean}(||\mathbf{z}_k||) + \min \mathbf{x}^f. \end{aligned} \tag{21}$$

The mean of the angle is corrected to ensure that it is not affected by the discontinuity in the unit circle. Then we convert the point to cartesian coordinates according to

$$\mathbf{x}^c = r^c \begin{bmatrix} \cos(\theta^c) \\ \sin(\theta^c) \end{bmatrix}, \tag{22}$$

This means that if either constraint is violated, $\mathbf{x}^c$ will be initiated behind the wall of sensor measurements generated by the object contour. There is also a local optimum relating to the heading. In particular, $\phi + \pi$, i.e., the reverse heading, is a local optimum since it is also aligned with the symmetry axis defined by the covariance function. To avoid this local optimum, we can utilize the velocity vector to design a similar constraint for the heading as for the centroid, i.e., ϕ is initialized according to the following criteria:

$$\phi = \begin{cases} \phi & \text{if } (\phi - \operatorname{atan2}(\dot{y}^p, \dot{x}^p)) < \pi/3 \\ \operatorname{atan2}(\dot{y}^p, \dot{x}^p) & \text{if } (\phi - \operatorname{atan2}(\dot{y}^p, \dot{x}^p)) \geq \pi/3 \end{cases}. \tag{23}$$

This scheme will not be applicable in all cases, e.g., reversing targets or surface vessels that drift with a strong current, but for most cases where tracking targets is relevant, this condition will be applicable.

B. Negative Information

In [14], the concept of negative information is used to constrain the bounds of the estimated extent so that it doesn't expand beyond the received measurements. This is achieved by estimating the minimum and maximum angles of the extended object and comparing these to the minimum and maximum angles of the actual measurements associated with that object. The minimum and maximum angles of the measurement set are therefore used as an additional measurement; these measurements are termed virtual measurements. A generic measurement equation for these virtual measurements can be written as

$$\begin{aligned} \max \angle \mathbf{z}_k &= h_k^{max}(\mathbf{x}_k) + \eta_k^{max}, \qquad \eta_k^{max} \sim \mathcal{N}(0, \mathbf{R}_k^{max}) \\ \min \angle \mathbf{z}_k &= h_k^{min}(\mathbf{x}_k) + \eta_k^{min}, \qquad \eta_k^{min} \sim \mathcal{N}(0, \mathbf{R}_k^{min}). \end{aligned} \tag{24}$$

We use the same approach, but we perform the state estimation utilizing the IEKF framework presented above.

The key assumption that allows us to perform the state estimation in the IEKF framework is to assume that, for the GP target model, the minimum and maximum angles of an extended object are achieved by sampling points of the extent, i.e., one of the elements of Θ^f. Then, we can derive an expression for these points in global coordinates since we can calculate the global position of each test point from the following expression:

$$\mathbf{x}_G^f = \mathbf{x}_k^c + \mathbf{x}_k^f \begin{bmatrix} \cos\left(\Theta^f + \phi_k\right) \\ \sin\left(\Theta^f + \phi_k\right) \end{bmatrix}. \tag{25}$$

We can then calculate the minimum and maximum angles that the extended object occupies

$$\begin{aligned} \kappa_{min} &= \min \angle \mathbf{x}_G^f \\ \kappa_{max} &= \max \angle \mathbf{x}_G^f. \end{aligned} \tag{26}$$

This allows us to determine the angular sector that an extended object occupies. These relations are presented graphically in Fig. 2. To define the measurement equation for these angles, we define

$$\begin{aligned} \theta_{max}^{(L)} &= \theta_{max}^f \\ \theta_{max}^{(G)}(\phi_k) &= \angle\left(\mathbf{x}_G^f - \mathbf{x}_k^c\right) = \theta_{max}^f + \phi_k, \end{aligned} \tag{27}$$

where θ_{max}^f is the element of Θ^f which corresponds to κ_{max}, which can be defined both in the local target frame (L) and the global frame (G). The time index k has been omitted from θ for notational convenience. With these definitions, we can compute the points to the extent that correspond most closely to the measurements with the maximum and minimum angles using (14)

$$\mathbf{z}_k^{max} = \mathbf{x}_k^c + \mathbf{p}_k(\theta_{max}^{(G)}(\phi_k))\mathbf{H}^{\mathbf{f}}\left(\theta_{max}^f\right)\mathbf{x}_k^f. \tag{28}$$

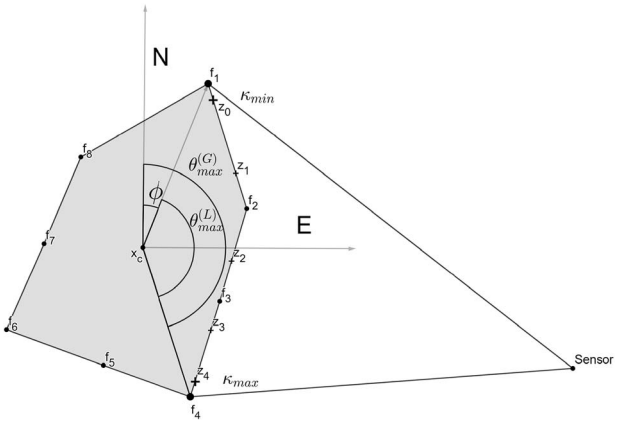

Figure 2. The extreme angles of the extended object κ_{min} and κ_{max} are given by the points f_1 and f_4, respectively, which are equivalent to $\mathbf{x}_G^f$ calculated for the 1st and 4th test point. The angles given by measurements z_0 and z_4 are the virtual measurements, and κ_{min} and κ_{max} are the corresponding predicted virtual measurements.

Utilizing this expression, we can calculate the global angle of these points

$$\begin{aligned} h_k^{max}(\mathbf{x}_k) &= \angle \mathbf{z}_k^{max} \\ &= \operatorname{atan2}\left(\frac{y_k^p + \sin(\theta_{max}^{(G)}(\phi_k))\mathbf{H}^{\mathbf{f}}\left(\theta_{max}^f\right)\mathbf{x}_k^f}{x_k^p + \cos(\theta_{max}^{(G)}(\phi_k))\mathbf{H}^{\mathbf{f}}\left(\theta_{max}^f\right)\mathbf{x}_k^f}\right). \end{aligned} \tag{29}$$

For the minimum angle, substitute θ_{max}^f for θ_{min}^f. The measurement Jacobian for this equation can be found by calculating the partial derivatives; see Appendix A for the applicable expressions. The noise component should also be transformed to extract the angular component. However, since we have chosen θ_{max}^f to be a test point, there is no uncertainty from the GP regression [22], $\mathbf{R}^f = 0$, and we are simply left with the noise component of the measurement, which we can define as

$$\mathbf{R}_k^{max} = \sigma_\kappa^2, \tag{30}$$

where σ_κ is the standard deviation of the angular component of the measurement noise. The actual measurements, which are used as virtual measurements, can be found by finding the measurements with the minimum and maximum angles. These virtual measurements are then used to augment the quantities in (11) such that

$$\begin{aligned} \mathbf{z}_k^* &= [\mathbf{z}_k, \quad \max \angle \mathbf{z}_k, \quad \min \angle \mathbf{z}_k]^\mathsf{T} \\ \mathbf{R}_k^* &= \operatorname{diag}\left[\mathbf{R}_k, \quad \mathbf{R}_k^{max}, \quad \mathbf{R}_k^{min}\right] \\ \mathbf{h}_k^*(\mathbf{x}_k) &= \left[\mathbf{h}_k(\mathbf{x}_k), \quad h_k^{max}(\mathbf{x}_k), \quad h_k^{min}(\mathbf{x}_k), \right]^\mathsf{T}, \end{aligned} \tag{31}$$

where $\mathbf{z}_k, \mathbf{R}_k$, and $\mathbf{h}_k(\mathbf{x})$ are defined by (11). Correspondingly, we can define a new cost function as

$$q(\boldsymbol{\xi}) = \left(\begin{bmatrix} \mathbf{z}_k^* \\ \hat{\mathbf{x}} \end{bmatrix} - \begin{bmatrix} \mathbf{h}^*(\boldsymbol{\xi}) \\ \boldsymbol{\xi} \end{bmatrix}\right)^\mathsf{T} \begin{bmatrix} \mathbf{R}^* & 0 \\ 0 & \mathbf{P} \end{bmatrix}^{-1} \left(\begin{bmatrix} \mathbf{z}_k^* \\ \hat{\mathbf{x}} \end{bmatrix} - \begin{bmatrix} \mathbf{h}^*(\boldsymbol{\xi}) \\ \boldsymbol{\xi} \end{bmatrix}\right). \tag{32}$$

This ensures that the virtual measurements are included in the GN optimization.

Table I
GP Update Algorithm

Input: Predicted state and covariance $\mathbf{x}_{k|k-1}, \mathbf{P}_{k|k-1}$, Associated measurements Z_C
Output: Updated state and covariance $\hat{\mathbf{x}}_k, \mathbf{P}_k$, Measurement likelihood l_C
if Equation (20) **and** $|Z_C| \geq 2$ **then**
  $\mathbf{x}_{iter} \leftarrow \mathbf{x}_{k|k-1}$ modified by Equations (22) and (23)
else
  $\mathbf{x}_{iter} \leftarrow \mathbf{x}_{k|k-1}$
end if
if $|Z_C| \geq 2$ **and not** partialOcclusion **and** $\mathbf{x}_{iter} \neq \mathbf{x}_{k|k-1}$ **then**
  negativeInformation = True
else
  negativeInformation = False
end if
$i \leftarrow 0$
while $i \leq GPMaxIterations$ **and** $eps > 10^{-4}$ **do**
  $\mathbf{x}_{upd} \leftarrow$ SingleGPUpdate$(\mathbf{x}_{k|k-1}, \mathbf{x}_{iter}, \mathbf{P}_{k|k-1}, Z_C)$
  $eps \leftarrow \mathbf{x}_{iter} - \mathbf{x}_{upd}$
  $\mathbf{x}_{iter} \leftarrow \mathbf{x}_{upd}$
  $i \leftarrow i + 1$
  if $i > GPMaxIterations$ **and** NegativeInformation **and** $(eps > 10^{-4}$
    or $\dot{\phi}_{upd} > \pi/4)$ **then**
    $i \leftarrow 0$
    $eps \leftarrow 10^3$
    $\mathbf{x}_{iter} \leftarrow \mathbf{x}_{k|k-1}$
    NegativeInformation = False
  end if
end while
$\mathbf{x}_k \leftarrow \mathbf{x}_{upd}$
Update covariance $\mathbf{P}_k$
Update α and β according to (18)
Calculate measurement set likelihood l_C via (41)

Table II
SingleGPUpdate

Input: Predicted state and covariance $\mathbf{x}_{k|k-1}, \mathbf{P}_{k|k-1}$,
  Current state $\mathbf{x}_{iter}$, Associated measurements Z_C
Output: Updated state $\mathbf{x}_{upd}$
for all $z \in Z_C$ **do**
Evaluate equation (14) with $\mathbf{x}_{iter}$
end for
Construct $\mathbf{H}_k, \mathbf{R}_k, \mathbf{h}(\mathbf{x})$ via equation (11)
if NegativeInformation **then**
$\kappa_{min/max} \leftarrow$ via equation (26)
Evaluate equation (29) and augment $\mathbf{H}_k, \mathbf{R}_k, \mathbf{h}(\mathbf{x}), \mathbf{z}_k$ with result
end if
$\mathbf{S}_k \leftarrow \mathbf{H}_k \mathbf{P}_{k|k-1} \mathbf{H}_k^{\mathrm{T}} + \mathbf{R}_k$
$\mathbf{W}_k \leftarrow \mathbf{P}_{k|k-1} \mathbf{H}_k^{\mathrm{T}} \mathbf{S}_k^{-1}$
$\mathbf{x}_{upd} \leftarrow \mathbf{x}_{k|k-1} + \mathbf{W}_k \left((\mathbf{z}_k - \mathbf{h}(\mathbf{x})) - \mathbf{H}_k (\mathbf{x}_{k|k-1} - \mathbf{x}_{iter}) \right)$

1) Practical Considerations: We only generate these virtual measurements if we have at least two measurements; otherwise, the virtual measurements will be identical, which implies a very small extent and will have the practical effect of shrinking extents. Incorporating these virtual measurements can be viewed as further constraining the optimization problem. In some cases, this can prevent convergence of the iterative optimization, and this is usually not desirable. Therefore, if the optimization does not converge while using virtual measurements, we repeat the optimization without including them in the cost function. Similarly, the use of virtual measurements has a tendency to estimate a rather large rotation of the extent in certain situations, which can be seen as another undesirable local optimum. We therefore also repeat the optimization without virtual measurements if the estimated rotational velocity is higher than a certain threshold. We also do not use virtual measurements when the initialization criteria in (20) and (23) are used, as convergence is harder to achieve in that case. The full method is summarized in algorithmic form in Tables I and II.

IV. THE GP-PMBM TRACKER

Given the state space model presented above, we now provide the specific closed-form expressions for the PMBM filter recursions for the GP model based on the general form given in [3]. We then discuss specific considerations for using the GP model in the PMBM framework and present the approximations used to make the tracker computationally feasible. Finally, we present the way occlusion is modeled using the information given by the virtual measurements in the previous section.

A. PMBM Filter Recursions with a GP Target Model

For the special case where the probability of survival P_S is constant and the following holds:

$$\begin{aligned} D_{k-1}^u(\mathbf{x}) &= \sum_{n=1}^{N_u} d_n^u \mathcal{N}(\mathbf{x}; \mathbf{x}_n^u, \mathbf{P}_n^u) \mathcal{G}(\alpha_n^u, \beta_n^u) \\ f_{k-1}^{j,i}(\mathbf{x}) &= \mathcal{N}(\mathbf{x}; \mathbf{x}_{k-1}^{j,i}, \mathbf{P}_{k-1}) \mathcal{G}(\alpha_{k-1}^{j,i}, \beta_{k-1}^{j,i}) \\ \mathbf{g}_{k|k-1}(\mathbf{x}|\mathbf{x}') &= \mathcal{N}(\mathbf{x}; \mathbf{F}\mathbf{x}', \mathbf{Q}), \end{aligned} \tag{33}$$

i.e., the probability distribution representing the target state in the Bernoulli components is a gamma-Gaussian distribution, and the PPP intensity is a linear combination of gamma-Gaussian distributions, i.e., a gamma-Gaussian mixture. The state transition density for the Gaussian and the gamma component is assumed to be independent, which enables separate prediction of the state and extent from the measurement rate. This assumption was used in [24]. The closed-form expression is then given by

$$\begin{aligned} D_{k|k-1}^u(\mathbf{x}) &= D^b(\mathbf{x}) \\ &\quad + P_S \sum_{n=1}^{N_u} d_n^u \mathcal{N}(\mathbf{x}; \mathbf{F}\mathbf{x}_n^u, \mathbf{F}\mathbf{P}_n^u\mathbf{F}^T + \mathbf{Q}) \mathcal{G}(\alpha_n^u, \beta_n^u) \\ w_{k|k-1}^j &= w_k^j \\ r_{k|k-1}^{j,i} &= r_k^{j,i} P_S \\ f_{k|k-1}^{j,i} &= \mathcal{N}(\mathbf{x}; \mathbf{F}\mathbf{x}_{k-1}^{j,i}, \mathbf{F}\mathbf{P}_{k-1}^{j,i}\mathbf{F}^T + \mathbf{Q}) \\ &\quad \times \mathcal{G}(\alpha_{k|k-1}^{j,i}, \beta_{k|k-1}^{j,i}). \end{aligned} \tag{34}$$

For the update step, we define the following predicted set densities

$$f^{j,i}_{k|k-1}(\mathbf{x}) = \mathcal{N}(\mathbf{x}; \mathbf{x}^{j,i}_{k|k-1}, \mathbf{P}^{j,i}_{k|k-1})\mathcal{G}(\alpha^{j,i}_{k|k-1}, \beta^{j,i}_{k|k-1})$$
$$D^{u}_{k|k-1}(\mathbf{x}) = \sum_{n=1}^{N_u} d^u_n \mathcal{N}(\mathbf{x}; \mathbf{x}^u_n, \mathbf{P}^u_n)\mathcal{G}(\alpha^u_n, \beta^u_n). \quad (35)$$

For a nonempty set of measurements Z_C conditioned on a target $\mathbf{x}$, the extended object measurement set likelihood [3] is given by

$$l(Z_C|\mathbf{x}) = P_D e^{-\lambda_m} \lambda_m^{|Z_C|} \prod_{\mathbf{z}\in Z_C} l(\mathbf{z}|\mathbf{x}). \quad (36)$$

$l(\mathbf{z}|\mathbf{x})$ is the single measurement likelihood, which in our case is given by the GP target model, i.e., (14). Due to the non-linearity of the measurement model, we make the following assumption:

$$l(\mathbf{z}^l|\mathbf{x}) \approx \mathcal{N}(\mathbf{z}^l; \mathbf{h}^l(\mathbf{x}), \mathbf{R}^l) \approx \mathcal{N}(\mathbf{z}^l; \mathbf{H}^l\mathbf{x}, \mathbf{R}^l), \quad (37)$$

i.e., $\mathbf{h}(\mathbf{x})$ defined in (14) is approximated by linearization with the jacobian matrix $\mathbf{H}^l$. With this, the product of the single measurement likelihoods can be written as

$$\mathcal{N}(\mathbf{z}; \mathbf{H}\mathbf{x}, \mathbf{R}) = \prod_{\mathbf{z}^l\in Z_C} \mathcal{N}(\mathbf{z}^l; \mathbf{H}^l\mathbf{x}, \mathbf{R}^l). \quad (38)$$

Here, $\mathbf{z}$ and $\mathbf{R}$ correspond to the augmented vectors and matrices defined in (11) for all measurements in the set Z_C and $\mathbf{H}$ is the concatenation of all matrices $\mathbf{H}^l$ given by these measurements. This is the joint likelihood of all the measurements in the set Z_C. Furthermore, to incorporate virtual measurements, we define the following:

$$\mathcal{N}(\mathbf{z}^*; \mathbf{H}^*\mathbf{x}, \mathbf{R}^*) = \mathcal{N}(\mathbf{z}; \mathbf{H}\mathbf{x}, \mathbf{R})\times$$
$$\mathcal{N}(\max\angle\mathbf{z}; \mathbf{H}^{max}\mathbf{x}, \mathbf{R}^{max})\mathcal{N}(\min\angle\mathbf{z}; \mathbf{H}^{min}\mathbf{x}, \mathbf{R}^{min}), \quad (39)$$

where $\mathbf{z}^*$ and $\mathbf{R}^*$ are defined in (31) and $\mathbf{H}^*$ is the linearization of $\mathbf{h}^*_k(\mathbf{x}_k)$. This is the joint likelihood of all measurements in the set Z_C if virtual measurements are incorporated. Given this, we can write the extended object measurement set likelihood as

$$l(Z_C|\mathbf{x}) = P_D e^{-\lambda_m} \lambda_m^{|Z_C|} \mathcal{N}(\mathbf{z}^*; \mathbf{H}^*\mathbf{x}, \mathbf{R}^*). \quad (40)$$

Using this, we can define the likelihood of a measurement set belonging to a measurement cell C conditioned on a given target estimate as

$$l_C(\alpha, \beta, \hat{\mathbf{x}}, \mathbf{P}, Z_C) = P_D \frac{\Gamma(\alpha + |Z_C|)\beta^\alpha}{\Gamma(\alpha)(\beta+1)^{(\alpha+|Z_C|)}|Z_C|!} \times \mathcal{N}(\mathbf{z}^*; \mathbf{H}^*\hat{\mathbf{x}}, \mathbf{S}^*), \quad (41)$$

where $\hat{\mathbf{x}}$ is the estimated mean of the target and the innovation covariance $\mathbf{S}^*$ is given by a Kalman filter update step and is as such defined by the matrices $\mathbf{H}^*$, $\mathbf{R}^*$, and the predicted covariance $\mathbf{P}$ corresponding to the target estimate. It is again assumed that the measurement rate and the combined state and extent are independent. The predicted likelihood of the gamma component was derived in [24]. We assume that the probability of detection P_D can be approximated as

$$P_D(\mathbf{x})p(\mathbf{x}) \approx P_D(\hat{\mathbf{x}})p(\mathbf{x}), \quad (42)$$

where $p(\mathbf{x})$ is a generic gamma-Gaussian probability distribution and $\hat{\mathbf{x}}$ is the mean of that distribution. This assumption holds trivially when $P_D(\cdot)$ is constant and is expected to hold when it is a sufficiently smooth function within the uncertainty area of the estimate [3]. With these definitions, we can state the following closed-form expressions. The PPP component representing undetected targets is updated as

$$D^u_k(\mathbf{x}) = Q_D D^u_{k|k-1}(\mathbf{x}), \quad (43)$$

i.e., the weight of each undetected target in the mixture is updated with the effective probability of a missed detection, defined as

$$Q_D = 1 - P_D + P_D e^{-\lambda_m}, \quad (44)$$

where the exponential term is the Poisson probability of a target generating no detections, this is equivalent to the likelihood of an empty set of measurements. The MBM is updated based on the associations made of measurements to measurement cells. The weights for the association hypotheses are updated as

$$w^{j,A}_k = \frac{w^j_{k|k-1}\prod_{C\in A} L^j_C}{\sum_{j\in\mathbb{J}_{k|k-1}}\sum_{A\in\mathcal{A}_j} w^j_{k|k-1}\prod_{C\in A} L^j_C}, \quad (45)$$

i.e., the weight of an association hypothesis A is given by a product of the likelihoods L of all measurement cells, normalized over all association hypotheses.

The updated parameters for the Gaussian distributions are given by a Kalman filter update step, and the updated gamma parameters for a measurement cell are given by (18). This corresponds to applying the steps in Table I.

The form of the update step for measurement cell C depends on if the measurement cell is associated with a detected or undetected target. The current time index k is omitted for brevity. For detected targets, we have two cases to consider

$$L^j_C = \begin{cases} 1 - r^{j,i_C}_{k|k-1} + r^{j,i_C}_{k|k-1}Q_D & |Z_C| = 0 \\ r^{j,i_C}_{k|k-1} l_C(\alpha^{j,i_C}, \beta^{j,i_C}, \hat{\mathbf{x}}^{j,i_C}, \mathbf{P}^{j,i_C}, Z_C) & |Z_C| \neq 0 \end{cases}$$

$$r^{j,i_C}_k = \begin{cases} \frac{r^{j,i_C}_{k|k-1}Q_D}{1 - r^{j,i_C}_{k|k-1} + r^{j,i_C}_{k|k-1}Q_D} & |Z_C| = 0 \\ 1 & |Z_C| \neq 0 \end{cases}$$

$$f^{j,i_C}_k(\mathbf{x}) = \begin{cases} \mathcal{N}(\mathbf{x}; \mathbf{x}^{j,i_C}_{k|k-1}, \mathbf{P}^{j,i_C}_{k|k-1})\mathcal{G}(\alpha^{j,i_C}, \beta^{j,i_C}) & |Z_C| = 0 \\ \mathcal{N}(\mathbf{x}; \hat{\mathbf{x}}^{j,i_C}, \mathbf{P}^{j,i_C})\mathcal{G}(\alpha^{j,i_C}, \beta^{j,i_C}) & |Z_C| \neq 0 \end{cases}. \quad (46)$$

If measurements are assigned to undetected targets, there are also two cases to consider, since it is assumed that a cell containing more than one measurement cannot be clutter-originated. Note that the result is a component of the MBM since the target has now been detected.

For the following, we define $l_C = l_C(\alpha_n^u, \beta_n^u, \hat{\mathbf{x}}_n^u, \mathbf{P}_n^u, Z_C)$:

$$L_C^j = \begin{cases} D^c + \sum_{n=1}^{N^u} d_n^u l_C & |Z_C| = 1 \\ \sum_{n=1}^{N^u} d_n^u l_C & |Z_C| > 1 \end{cases}$$

$$r_k^{j,i_C} = \begin{cases} \frac{\sum_{n=1}^{N^u} d_n^u l_C}{D^c + \sum_{n=1}^{N^u} d_n^u l_C} & |Z_C| = 1 \\ 1 & |Z_C| > 1 \end{cases} \tag{47}$$

$$f_k^{j,i_C}(\mathbf{x}) = \sum_{n=1}^{N^u} d_n^u \mathcal{N}(\mathbf{x}; \hat{\mathbf{x}}_n^u, \hat{\mathbf{P}}_n^u) \mathcal{G}(\alpha_n^u, \beta_n^u).$$

See Appendix B for a derivation of these expressions.

B. Initialization and Birth Process

The GP model is generally not observable, especially with few measurements. Therefore, there is no unique solution, and the solution depends on the choice of prior used to initialize the estimate. The choice of prior is therefore of key importance. In particular, the general characteristics of the extent prior and the prior value of the heading need to be specified. In the PMBM framework, the prior estimates are encoded in the birth process intensity D^b. Using the mixture representation of the PPP intensity function, i.e.,

$$D^b(\mathbf{x}) = \sum_{n=1}^{N^b} w_n^b p_n^b(\mathbf{x}), \tag{48}$$

we can define several priors, and since the weight of the PPP components will be updated based on the likelihood of the measurements, the resulting estimate will be weighted. Selecting these priors is still not a trivial choice and, in most cases, are tuned to fit the particular problem. For instance, in [15] where a GP model was used to track vehicles, the prior for the extent ($\mathbf{x}_0^{\mathbf{f}}$) was chosen to correspond to the extent of a real vehicle.

In this work, we use a similar method to the one that was used to define a birth density along the edge of the surveillance area in [18]. We assume an expected maximum range of the sensor R^b, and use it to set the positional component of the birth process intensity. Given N^b components, an angle for each component is defined as $\psi_n^b = \frac{n2\pi}{N^b}$. The prior for the centroid is then given by

$$\mathbf{x}_n^c = R^b \begin{bmatrix} \cos\psi_n^b \\ \sin\psi_n^b \end{bmatrix}, \tag{49}$$

i.e., spread the mixture components uniformly on or slightly beyond the edge of the circle defined by the maximum range of the sensor. By placing it beyond, the centroid will be placed behind the first measurements. The heading can be defined by

$$\phi_n^b = \psi_n^b + \pi, \tag{50}$$

i.e., the direction toward the sensor. The direction of the velocity vector can be defined similarly along with a predefined magnitude v^b, i.e.,

$$\dot{\mathbf{x}}_n^c = v^b \begin{bmatrix} \cos\phi_n^b \\ \sin\phi_n^b \end{bmatrix}. \tag{51}$$

The angular velocity $\dot{\phi}_n^b$ can be assumed to be 0 rad/s. The covariance of all these kinematic states is inflated to ensure that the mixture components can represent a variety of states. With regards to the extent, it should be tailored to the targets that are expected to appear. In this case, because we are tracking ships, we define the extent prior as a ship-like shape with a pointed bow and a flat stern with symmetry along the vertical axis. If it is desirable to track targets with very different shapes, one can also include different shapes in the birth intensity function.

C. Mixture Reduction

Mixture reduction is also a necessary tool used in the birth process to reduce all the components in the PPP mixture into one Bernoulli. It can also be used to merge Bernoullis that are similar. The merging is done using standard Gaussian mixture reduction for the kinematic and extent states and by the method derived in [24] for the parameters of the gamma distribution.

D. Reducing Associations

To reduce the number of data associations, gating is performed as an initial step. Gating for the GP model was presented in the original paper presenting the model [11], and the same method is used in this work. This separates the targets and measurements into independent subgroups. Further reduction of association hypotheses is done using the stochastic optimization method presented in [6] to find the most likely associations. As an implementational detail, we calculate the predicted measurement and the measurement matrix for each measurement-object pair once during the gating process and store them for use during the stochastic optimization method to avoid redundant computation of (14), which involves one GP regression per measurement, a relatively expensive computation.

E. Occlusion

To utilize negative information for state estimation in a multiobject framework, we have to account for the occluding effect of other targets. A natural choice to model occlusion would be to modify the probability of detection P_D. For multiple extended object tracking, this has been done in [18] and further modified in [19]. They used the GIW model and calculated a probability of detection based on the angles occupied by each target and their distance to the sensor. Partial occlusion was handled by discretizing each point on the extent of a target, calculating the probability of detection for each point,

and taking the maximum as the probability of detection for that target. This method was reused in the PMBM framework in [3]. Another approach was presented in [20], which calculates an occlusion likelihood based on the current targets. This occlusion likelihood is represented by a Gaussian mixture that can be used to update the state of undetected objects, infer the existence of objects, and inform the association of data.

The zone being occluded by a specific object is given by the angles occupied and the distance of the object from the sensor which we define as $(\kappa^i_{min}, \kappa^i_{max}, \rho^i)$. In [20], this is expressed as a combination of the following conditions. Object i is fully occluded by object i_O if the following conditions are true

$$\begin{aligned} B &= (\kappa^i_{min} \geq \kappa^{i_O}_{min}) \cap (\kappa^{i_O}_{max} \geq \kappa^i_{max}) \\ R &= (\rho^i \geq \rho^{i_O}). \end{aligned} \tag{52}$$

Condition B can be referred to as the bearing condition and condition R can be referred to as the radial condition. An object is partially occluded if either of the following bearing conditions are true in combination with the radial condition R

$$\begin{aligned} B_{min} &= (\kappa^{i_O}_{max} \geq \kappa^i_{max}) \cap (\kappa^i_{max} \geq \kappa^{i_O}_{min}) \\ B_{max} &= (\kappa^{i_O}_{max} \geq \kappa^i_{min}) \cap (\kappa^i_{min} \geq \kappa^{i_O}_{min}). \end{aligned} \tag{53}$$

Figure 3 shows an example where these cases occur. With this, we can define the probability of a target i being occluded by another target i_O as

$$P^{i,i_O}_O = p(B, R, E) = p(B|E)p(R|E)p(E), \tag{54}$$

where $p(B|E)$ and $P(R|E)$ is the probability of the conditions of (52) being true conditional on the existence of target i_O and $p(E) = r^{i_O}$, i.e., the probability of existence of target i_O. For partial occlusion, we can similarly state

$$P^{i,i_O}_{pO} = p(B_{max/min}, R, E) = p(B_{max/min}|E)p(R|E)p(E). \tag{55}$$

In [20], $(\kappa^i_{min}, \kappa^i_{max}, \rho^i)$ were all assumed Gaussian distributed. We can then calculate the resulting probability of the occlusion conditions by using the cumulative distribution function

$$p(B|E) = \Phi\left(\frac{\kappa^{i_O}_{max} - \kappa^i_{max}}{\sqrt{\sigma^2_{\kappa^{i_O}_{max}} + \sigma^2_{\kappa^i_{max}}}}\right) \Phi\left(\frac{\kappa^i_{min} - \kappa^{i_O}_{min}}{\sqrt{\sigma^2_{\kappa^{i_O}_{min}} + \sigma^2_{\kappa^i_{min}}}}\right), \tag{56}$$

where $\Phi(\cdot)$ is the cumulative distribution function of a Gaussian distribution with zero mean and unit variance; for more details, see [20]. Using the virtual measurements generated in the previous section, we can find a Gaussian distribution for κ^i_{min} and κ^i_{max} from (28) and calculate the resulting innovation variance for each virtual measurement according to

$$\begin{aligned} \sigma^2_{\kappa^i_{min}} &= \mathbf{H}^i_{min}\mathbf{P}^i{\mathbf{H}^i_{min}}^{\mathsf{T}} + \mathbf{R}^{min} \\ \sigma^2_{\kappa^i_{max}} &= \mathbf{H}^i_{max}\mathbf{P}^i{\mathbf{H}^i_{max}}^{\mathsf{T}} + \mathbf{R}^{max}. \end{aligned} \tag{57}$$

The probability of partial occlusion can be calculated in the same manner using the same terms, which becomes

$$\begin{aligned} p(B_{min}|E) &= \Phi\left(\frac{\kappa^{i_O}_{max} - \kappa^i_{min}}{\sqrt{\sigma^2_{\kappa^{i_O}_{max}} + \sigma^2_{\kappa^i_{min}}}}\right) \Phi\left(\frac{\kappa^i_{max} - \kappa^{i_O}_{max}}{\sqrt{\sigma^2_{\kappa^{i_O}_{max}} + \sigma^2_{\kappa^i_{max}}}}\right) \\ p(B_{max}|E) &= \Phi\left(\frac{\kappa^{i_O}_{min} - \kappa^i_{min}}{\sqrt{\sigma^2_{\kappa^{i_O}_{min}} + \sigma^2_{\kappa^i_{min}}}}\right) \Phi\left(\frac{\kappa^i_{max} - \kappa^{i_O}_{min}}{\sqrt{\sigma^2_{\kappa^{i_O}_{min}} + \sigma^2_{\kappa^i_{max}}}}\right). \end{aligned} \tag{58}$$

For ρ^i, we do not have an equivalent way to calculate a Gaussian distribution, so we instead define

$$p(R|E) = \begin{cases} 1 & \text{if} \quad ||\mathbf{x}^i|| > ||\mathbf{x}^{i_O}|| \\ 0 & \text{otherwise} \end{cases}. \tag{59}$$

With this, we can calculate the probability of occlusion for each target pair. Furthermore, with a PMBM framework, both the detected and undetected targets can be occluded, and therefore, we should calculate the probability of occlusion for both these sets. However, only detected targets will have an occluding effect.

Occlusion or partial occlusion have different effects on other model parameters. If we determine that a target

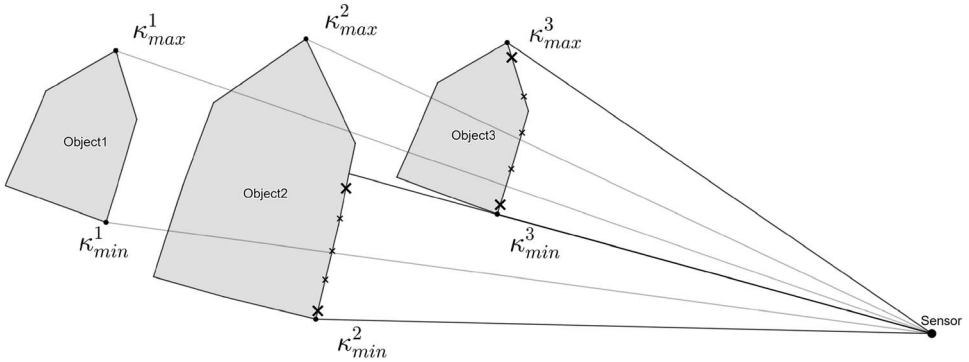

Figure 3. Three targets, where object 1 is occluded by object 2, which in turn is partially occluded by object 3. The angles κ are shown for each object. The measurements generated by the sensor are represented by crosses, and the measurements used for the virtual measurements are shown by the larger crosses.

is wholly occluded by another, the probability of detection will be lowered for that target. Taking the probability of occlusion into account therefore gives a target-specific probability of detection

$$P_D^i = P_D \prod_{i_O \in \mathbb{I}_O} (1 - P_O^{i,i_O}), \tag{60}$$

where $\mathbb{I}_O$ is the total set of occluding targets for target i. If the occlusion probability of any target is 1, then we will have $P_D = 0$; this will cause issues with likelihood calculations, so we enforce a minimum probability of detection. For a component of the PPP mixture u_n, the expression becomes

$$P_D^{u_n} = P_D \sum_{j \in \mathbb{J}} w_j \prod_{i_O \in \mathbb{I}_O^j} (1 - P_O^{u_n,i_O}), \tag{61}$$

i.e., the probability of detection of a component is a weighted average of the probability of detection for every hypothesis in the MBM.

F. Partial Occlusion

Partial occlusion will not affect the probability of detecting the target according to the model assumptions since the target will still generate measurements. However, it will affect the model parameters in other ways. The first is the way negative information is utilized for state estimation since partial occlusion will not match with the assumptions underlying the generation of the virtual measurements. Specifically, if the target is partially occluded, the expected angle κ will no longer correspond to either the minimum or maximum angles of the measurement set, depending on the part of the target that is occluded. In this work, we therefore do not utilize negative information for the state estimation when a target is partially occluded, but we note that it is possible to do so by calculating where κ would intersect on the target contour and use that in place of $\theta^f_{max/min}$ in the measurement equation for negative information. In addition, partial occlusion will affect the number of measurements that are generated by the objects, which will have an impact on the association likelihood in (41) since the gamma distribution will not be able to account for this. So this effect needs to be managed as well, and in this work, we do this by defining a heuristic visibility ratio

$$v^i = \frac{\min(\kappa^{i^{pO}}_{max}) - \max(\kappa^{i^{pO}}_{min})}{\kappa^i_{max} - \kappa^i_{min}}, \tag{62}$$

where $i^{pO} \in \mathbb{I}^{pO}$ are the partially occluding objects. Here, we simply consider the mean of κ, ignoring the uncertainty of each estimate. With this ratio, we also need to consider the probability of occlusion. We define a correction factor as

$$\eta_v^i = 1 - P^i_{pO}(1 - v^i). \tag{63}$$

The probability of occlusion becomes more complicated to calculate for multiple occluding objects since they will all occlude different sectors of the object; each part of an object's extent will therefore, in theory, have its own probability of occlusion. For the sake of simplicity, we utilize the maximum probability of occlusion of the objects partially occluding object i

$$P^i_{pO} = \max P^{i,i_O \in \mathbb{I}^{pO}}_{pO}. \tag{64}$$

Again, for the PPP component, the correction factor should also consider the weights of the MBM, giving the resulting expression

$$\eta_v^{u_n} = \sum_{j \in \mathbb{J}} w_j \eta_v^j, \tag{65}$$

where η_v^j is defined as the correction factor calculated for component u_n using the Bernoullis in the jth MBM. This correction factor is then utilized to modify the parameters of the gamma distribution. We assume that the Poisson rate of a partially occluded target is $\eta_v \lambda_m$, and recall that λ_m is gamma distributed with shape parameter α and inverse scale parameter β. Given this, the Poisson rate of a partially occluded target is gamma distributed with the following parameters:

$$\eta_v \lambda_m \sim \mathcal{G}\left(\alpha, \frac{\beta}{\eta_v}\right). \tag{66}$$

This is equivalent to scaling the gamma distribution since we have divided the inverse scaling parameter with our scaling factor η_v. We can express this in the existing gamma recursions as

$$\begin{aligned} &\alpha_{k|k-1} = \frac{\alpha_{k-1}}{\eta_\gamma}, \qquad \beta_{k|k-1} = \frac{\beta_{k-1}}{\eta_v \eta_\gamma} \\ &\alpha_k = \alpha_{k|k-1} + |Z_C|, \qquad \beta_k = \eta_v(\beta_{k|k-1} + 1). \end{aligned} \tag{67}$$

In this way, the parameters of the gamma distribution are in line with the number of measurements we expect to receive; in other words, the predictive likelihood of the expected number of measurements is preserved

$$\frac{\Gamma(\alpha_{k|k-1} + |Z_C|)\beta_{k|k-1}^{\alpha_{k|k-1}}}{\Gamma(\alpha_{k|k-1})(\beta_{k|k-1} + 1)^{(\alpha_{k|k-1}+|Z_C|)}|Z_C|!}. \tag{68}$$

1) Practical Considerations: The visibility ratio defined in (62) is only well defined between 0 and 1. However, it could take on values larger than 1 if the expressions are applied naively as stated. Therefore, we enforce the conditions in (53) explicitly. In the presence of full occlusion, the visibility ratio will become a negative value. In this case, we set the correction factor to 1. This is for practical reasons since a very low correction factor while not receiving any measurements for an extended period could cause the target estimate to be overly attracted to clutter.

The whole procedure for correcting for occlusion is presented in Table III. Finally, the complete update step for the GP-PMBM tracker is presented in Table IV.

Table III
Occlusion Correction

Input: A predicted PMBM
Output: A probability of detection P_D and a correction factor η_v for every component in the predicted PMBM
for $j \in \mathbb{J}$ **do**
for $i \in \mathbb{I}$ **do**
$(\kappa^i_{min}, \kappa^i_{max}) \leftarrow$ via Equation (26)
end for
for $i \in \mathbb{I} \cup D^u$ **do**
for $i_O \in \mathbb{I}_{\notin i}$ **do**
condmin $\leftarrow \kappa^{i_O}_{min} \leq \kappa^i_{min}$ **and** $\kappa^{i_O}_{max} \geq \kappa^i_{min}$
condmax $\leftarrow \kappa^{i_O}_{min} \leq \kappa^i_{max}$ **and** $\kappa^{i_O}_{max} \geq \kappa^i_{max}$
conddistance $\leftarrow ||\mathbf{x}^{\mathbf{c}i}|| > ||\mathbf{x}^{\mathbf{c}i_O}||$
if conddistance **then**
${P_O}^{i,i_O} \leftarrow$ via Equation (54)
end if
if condmin **and** condmax **and** conddistance **then**
$\eta_v \leftarrow 1$
else if not condmin **and** condmax **and** conddistance **then**
Save $\kappa^{i_O}_{max}$
Assign $i_O \in \mathbb{I}^{pO}$
${P_{pO}}^{i,i_O} \leftarrow$ via Equation (55)
else if condmin **and not** condmax **and** conddistance **then**
Save $\kappa^{i_O}_{min}$
Assign $i_O \in \mathbb{I}^{pO}$
${P_{pO}}^{i,i_O} \leftarrow$ via Equation (55)
end if
end for
Determine $\min(\kappa^{i^{pO}}_{max})$ and $\max(\kappa^{i^{pO}}_{min})$
$v^i \leftarrow$ via Equation (62)
$\eta^i_v \leftarrow$ via Equation (63)
$P^i_D \leftarrow$ via Equation (60)
end for
end for
$P^{u_n}_D \leftarrow$ via Equation (61)
$\eta^{u_n}_v \leftarrow$ via Equation (65)

Table IV
Full GP-PMBM Update

Input: A predicted Poisson Multi-Bernoulli Mixture and a measurement set Z
Output: An updated Poisson Multi-Bernoulli Mixture
Correct for occlusion via Table III
Perform gating for each component of the PMBM
for $j \in \mathbb{J}$ **do**
Compute most likely subset of associations $\mathcal{A}_j$
for $A \in \mathcal{A}_j$ **do**
for $C \in A$ **do**
if New Target **then**
for Each component of $D^u \in C$ **do**
Update component(s) via Table I
end for
$f^{j,i_C} \leftarrow$ via mixture reduction of component(s)
$L^j_C, r^{j,i_C} \leftarrow$ via Equation (47)
else if Existing Target **then**
$f^{j,i_C} \leftarrow$ via Table I
$L^j_C, r^{j,i_C} \leftarrow$ via Equation (46)
end if
end for
for Targets without Detection **do**
$f^{j,i_C}, L^j_C, r^{j,i_C} \leftarrow$ via Equation (46)
end for
end for
end for
Update weights via Equation (45)
Update D^u via Equation (43)

V. SIMULATION STUDY

In this section, we present the result from a Monte Carlo simulation study where the performance of the PMBM-tracker using the presented GP model is compared with the implementation using the GGIW model as presented in [5][1]. For the GP model, we present results without the negative information and occlusion handling as GP, and the results including those features are presented as GP-NI.

A. Simulation Scenario

The scenario consists of 8 ships that are born from timestep 1 to 50. The simulation area is 200×200 m in total with a sensor placed at the center, which has a measurement range of 100 m. Two vessels spawn from each side of the area and approach the center, where they turn. The scenario was particularly handcrafted to simulate occlusion, so that some vessels are born behind another vessel. When the vessels reach the center, they appear close together and are frequently wholly or partially occluded during this time, with vessels traveling alongside one another. See Fig. 4 for a view of the scenario. The scenario lasts for 240 timesteps, and each vessel persists for 190 timesteps. The extent is modeled by a ship that is 6 m long, 3 m wide, and has a pointed bow where the full width is achieved 2 m behind it. The measurements are generated by simulating an LiDAR with a simulated maximum range of 100 m, angular resolution 0.5°, and a modeled radial accuracy of 0.1 m. Measurements are only generated if they hit a simulated hull, and only one measurement is generated per angle, which simulates occlusion. In addition, clutter is generated using a PPP with $\lambda_c = 20$ and a uniform spatial distribution, but the clutter measurements are also corrected for occlusion. The results are averaged over 100 Monte Carlo simulation runs.

B. Parameters

The PMBM parameters are chosen as follows: probability of detection $P_D = 0.90$ for the standard model and $P_D = 0.99$ when occlusion is modeled, probability of survival $P_S = 0.95$, and clutter rate $\lambda_c = 20$. The gating probability is set at $P_G = 0.99$; the pruning parameters are 0.01 for the existence probability, 0.005 for PPP mixture components, and 0.005 for MBM components. Both target models use $\sigma_c = 0.2$ m as the noise parameter for the CV model and $\sigma_r = 0.1$ m for the measure-

[1]The implementation for the GGIW model was taken from github.com/yuhsuansia/Extended-target-PMBM-tracker, and this implementation was modified for use with the GP model

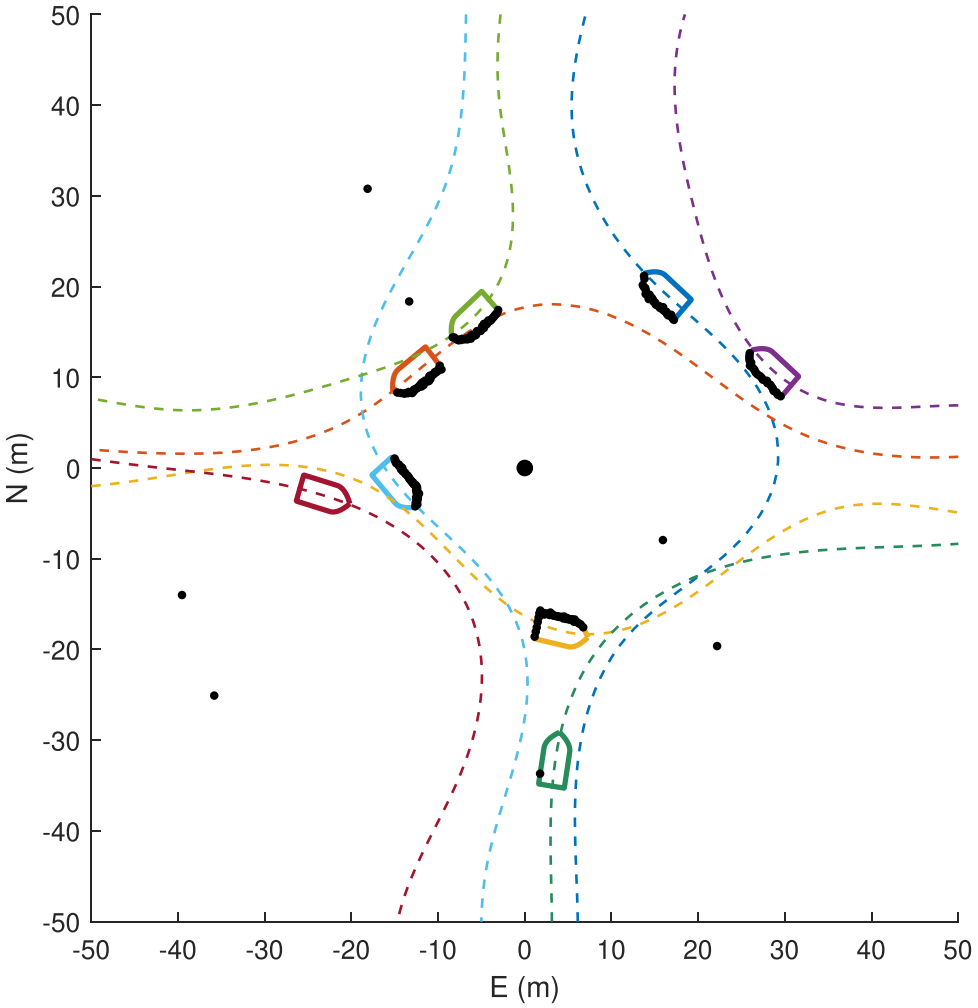

Figure 4. Visualization of the simulation scenario with the trajectories of all vessels, along with the ship extents and measurements visualized for timestep 105. Note that this does not show the whole simulation area but only the 100×100 m area in the center. The simulated LiDAR sensor is placed at the origin.

ment noise; the GP model uses $\sigma_\phi = 0.1$ rad as noise for the constant angular velocity model. For the virtual measurements, the measurement noise strength is $\sigma_\kappa = 0.5^\circ$, the same as the simulated sensor resolution. Both target models use $w_e = 20$ as the length of the gamma prediction window. For the GP target model, we use nine test angles to parametrize the extent, and the hyperparameters are $\sigma_f = 1.0$ m, $\sigma_r = 0.5$ m, $\sigma_n = 0.01$ m, $l = \pi/4$ rad and the forgetting factor $\eta_f = 0.001$. The maximum amount of IEKF iterations is 50. For the GGIW target model, we use 200 for the extent prediction window. The birth intensity function is defined according to the method defined above with $N^b = 36$ components and a range $R^b = 105$ m and a velocity magnitude of $v^b = 1$ m/s. The extent prior is roughly equivalent to the true extent for the GP model, and for the GGIW model, it is an ellipse with the same length and width defining the semi-axes; this is combined with the prior heading to calculate a prior value for the shape matrix X. The prior value of the gamma distribution is $\alpha_0 = 900$ and $\beta_0 = 100$. The covariance of the Gaussians is inflated to ensure coverage of the whole circle, the standard deviation of the positional component is 20 m, 3 m/s for the velocity component, and for the GP model the heading component is $\pi/4$ rad and the angular velocity is $\pi/4$ rad. In the case of the extent, for the GP model, the prior covariance is given by the covariance function.

C. Performance Evaluation

To compare the performance of the trackers, the generalized optimal sub-pattern assignment (GOSPA) metric [27] is used to provide a single metric for the performance of a multiobject tracking algorithm by incorporating localization error, missed targets, and false targets into a single metric. The parameters for the GOSPA metric were cut off $c = 10$ and power $p = 2$. To compare the extent estimates of the target models, we use the process of associating estimates to targets to generate additional measures that are comparable between them. One such measure is the Intersection-Over-Union (IOU) metric, which has been used in previous work to compare methods for extent estimation [11], [12]. To calculate the IOU metric for the GGIW model, the shape

Table V
Mean Value of Metrics for the Simulated Scenario

Model	GP	GP-NI	GGIW
GOSPA	9.52	**8.26**	11.40
Loc. Err.	5.47	**4.53**	11.07
Missed	1.55	**1.03**	1.91
False	0.33	0.48	**0.31**
IOU	0.59	**0.64**	0.33
Heading (rad)	0.40	**0.30**	1.75
Time (s)	**115.90**	158.96	118.19

The best values are highlighted in bold.

matrix X is decomposed to retrieve the length of the semi-axes, corresponding to the 2-σ ellipsoid, and the ellipse orientation. The heading error is calculated using the same method. Finally, the computation time for each run is also presented; however, it should be noted that the GP methods were made more computationally efficient by precomputing the measurement matrices during gating, which makes it hard to compare their computational times with that of the GGIW method, which does not have this implementation efficiency.

D. Results

The metrics are presented in Table V. Note the disparity of the IOU metric. This is primarily due to the inability of the GGIW model to model contour-generated measurements, since the GGIW model assumes a uniform distribution, and thus centers the ellipse on the contour instead, which causes large localization errors and large errors in extent estimation. Note also the larger heading error, showing an inability to estimate the heading as a separate state. We can also note the improvement in utilizing negative information and modeling occlusion as compared to the base GP method with the improvement in localization error and the IOU metric, as well as the reduction of the number of missed targets. However, it increases the number of false targets. The evolution of the metrics during the simulation run is shown in Fig. 5. It shows that the GGIW model has worse IOU and a worse localization error across the whole run, although the localization error is smaller while the ships are close to the sensor, due to the fact that the side of the vessel is measured rather than the front or rear. Comparing the regular method with the negative information method, we can note the disparity in the IOU metric starting around timestep 100, which is when occlusion occurs in the simulation, as well as the subsequent disparity in the localization error. This shows that the use of negative information results in an improved state estimate, particularly when targets are close together. The handling of occlusion also results in a notable improvement in the number of missed targets, due to the method being better at maintaining a track when occlusions occur, but the track is still lost for some targets due to occlusion. This is paired with an increase in false targets, particularly during the middle of the run, when a large part of the surveillance area is occluded by the targets. The reason for this could be that the way we model partial occlusion for undetected targets results in more erroneous detections due to clutter. With these results, we can state that the combination of modeling occlusion and negative information constitutes an improvement over the base GP method. However, it comes with an increase in computational time and false targets.

VI. TEST DATA

In this section, we present the result from real LiDAR data gathered from tests in Trondheim utilizing the two platforms milliAmpere and milliAmpere2 in the Trondheim canal [28].

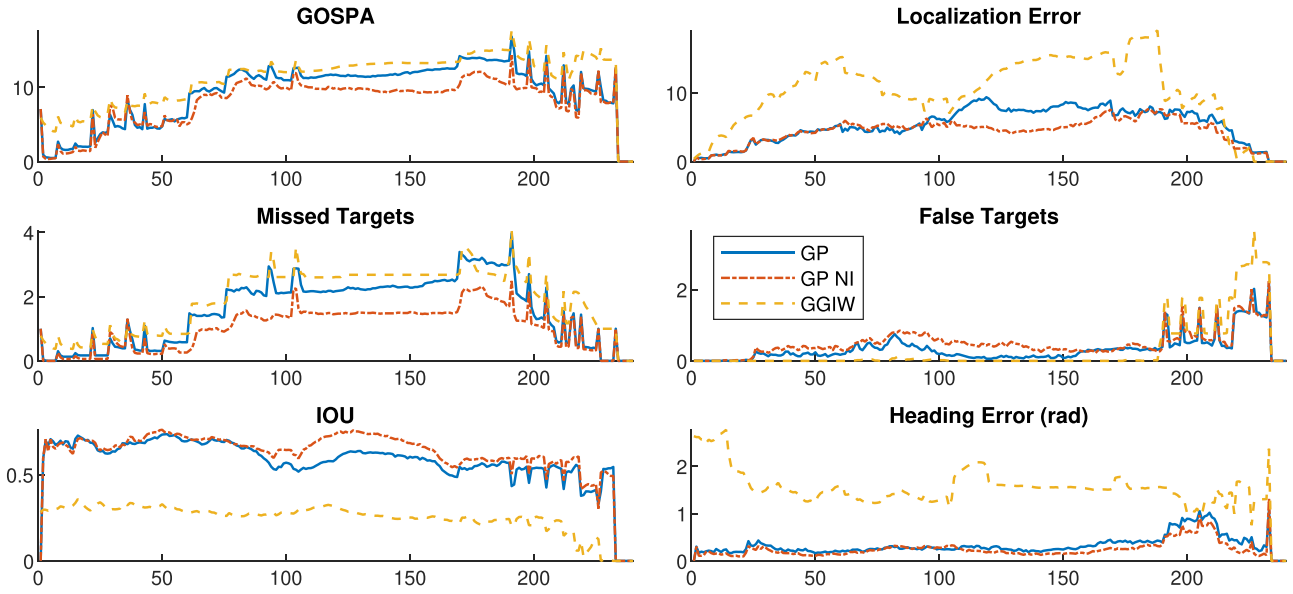

Figure 5. The evolution over the course of the simulation run for selected metrics as an average over all MC simulations.

A. Test Scenario

We present two separate scenarios, one with a single vessel performing maneuvers in front of the sensor in the canal (see Fig. 6a) and one with two vessels traveling in separate directions in the canal and passing each other (see Fig. 6b). The data from the first scenario was gathered using milliAmpere2, which is equipped with two Ouster OS1 32 LiDARs. These two point clouds were combined, and the returns from land and static obstacles along the canal were filtered out using manual land masking, and the point cloud was transformed to 2D by only retaining the point closest to the sensor in each angular resolution sector. The second scenario was published in [29] (as scenario 13) and is reused in this work.

B. Parameters

Most of the parameters used are similar to the simulation study. The range used to define the birth intensity R^b is reduced to 40 and 65 m, respectively, due to the observed range at which the LiDARs were able to detect the target vessels. For the second scenario, α_0 was set to 500 to account for the lower sensor resolution. The extent priors were set such that the length and width of the prior were roughly equivalent to the target vessels, but the same prior was used to represent both ships in the second scenario. In addition, some tweaks were made to attempt to mitigate some observed effects that are not modeled. To account for wake clutter, the clutter rate was increased to $\lambda_c = 60$ and $\lambda_c = 100$ for the first and second scenario, respectively. Finally, to account for errors related to sway affecting the pitch of the LiDAR sensor, the measurement noise σ_r was set to 0.5 m.

C. Performance Evaluation

We use the same metrics that were used in the simulation study, with the ground truth data gathered used to calculate the metrics. For the first scenario, ground truth was measured by using a dual antenna inertial navigation system (INS), and the extent of the vessel was measured to be able to compare the estimated extent with the ground truth. For the second scenario, the ground truth data gathered was only positional global navigation satellite system (GNSS) data without heading; in addition, the exact position of the GNSS receiver was unknown, which is a significant source of error for the IOU calculation. The heading was inferred from the velocity vector, which is also a source of error for the calculation of the IOU and heading error metrics.

Table VI
Mean Value of Metrics for the Real LiDAR Data

	Test 1			Test 2		
Model	GP	GP-NI	GGIW	GP	GP-NI	GGIW
GOSPA	1.51	**1.31**	2.45	4.76	**3.95**	4.06
Loc. Err.	0.85	**0.66**	1.80	4.81	3.68	**3.49**
Missed	0.08	**0.07**	**0.07**	**0.08**	0.08	0.10
False	0.00	**0.00**	0.01	0.01	0.00	**0.00**
IOU	0.36	**0.50**	0.12	0.20	0.26	**0.31**
Heading (rad)	0.37	**0.19**	1.30	0.46	**0.34**	1.86
Time (s)	**96.35**	111.51	161.31	256.53	257.85	**253.26**

The best values are highlighted in bold.

D. Results

The first scenario is quite simple from a target tracking perspective, it is simply a test of target birth and the ability of the target models to track the ship while it is performing complex maneuvers. The relevant metrics are presented in Table VI, and the plots are shown in Fig. 7. The GP model is able to track the target over the whole scenario. However, as the target gets closer to the sensor, the IOU value degrades; this is due to wake clutter being detected by the LiDAR around timestep 400. These wake measurements are associated with the

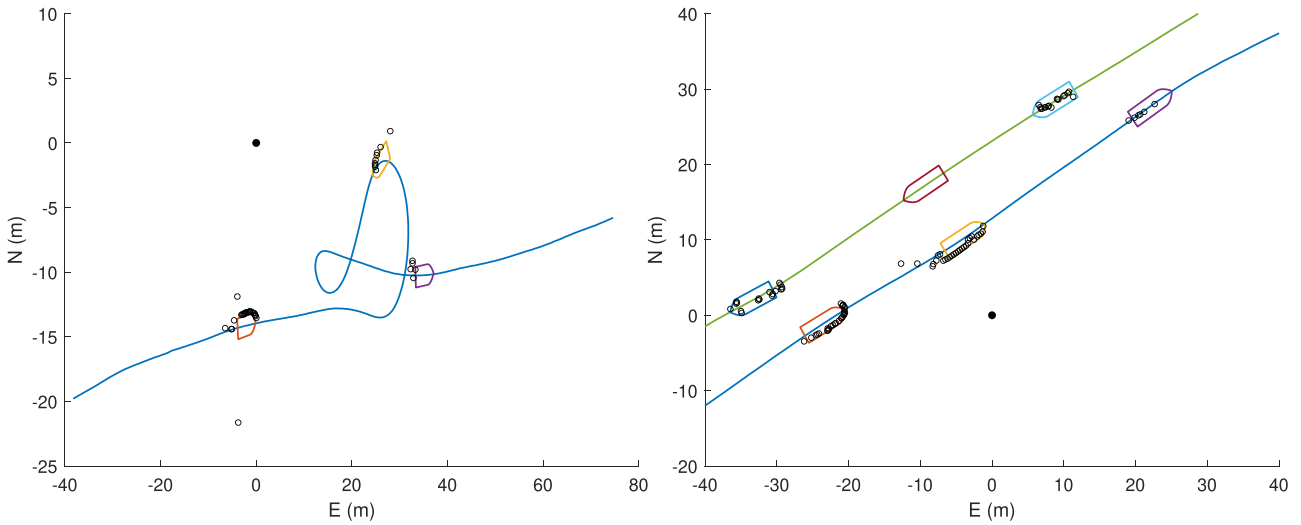

Figure 6. Visualization of the test scenarios, along with the extent and measurements visualized for three different timesteps, with the sensor platform placed at the origin. Note the measurements generated by the wake, as well as the occlusion in the second scenario.

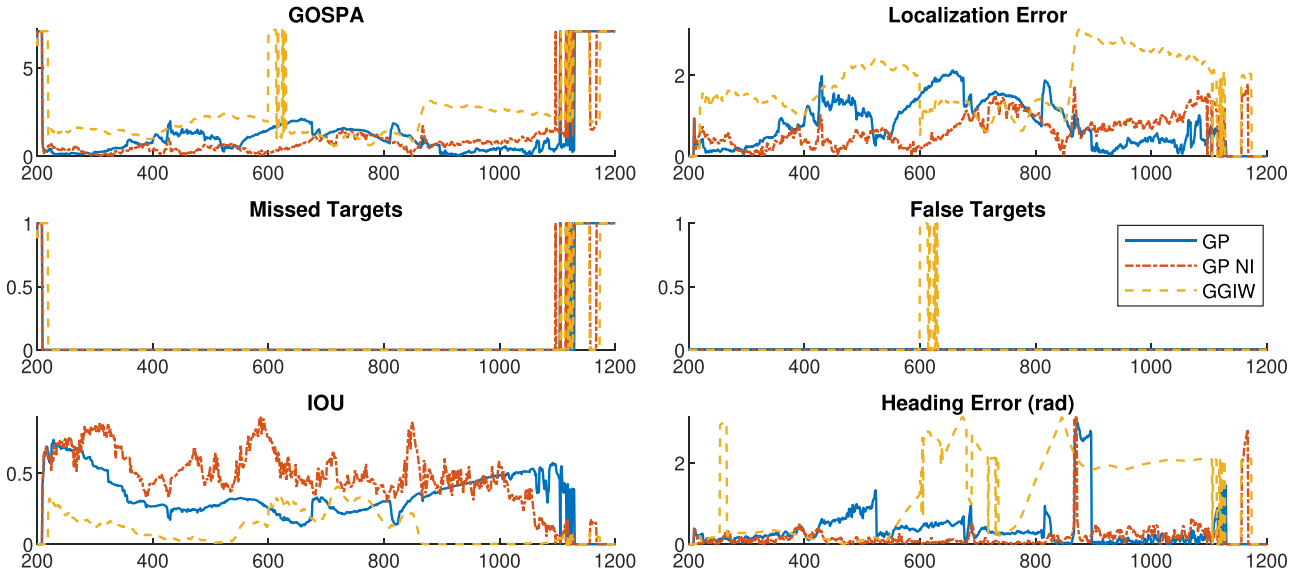

Figure 7. The evolution throughout the single target test run for selected metrics.

target because it does not adhere to the uniform clutter model. This affects the extent estimate and consequently the state estimate. The estimate is able to recover when the vessel completes a turn. In this case, utilizing negative information confers an improvement in the IOU and correspondingly in the localization error. This is due to the ability to more quickly adjust the extent estimate after being affected by the wake clutter, which we are able to do immediately due to the use of virtual measurements in the update step, whereas the base GP method cannot adjust the extent estimate if it is estimated as too large. The GGIW model initializes another track during one of the turning maneuvers to continue tracking the target, resulting in a false target for a few timesteps.

The second scenario is more complex, as it entails two targets, with one target being occluded by the other. The metrics are given in Table VI, and the evolution over time is shown in Fig. 8. Here, the base GP model performs worse compared to the GGIW model, with a higher localization error and lower IOU metric. This is due to the disruptive effect of wake clutter on the GP model, which causes the extent estimates to get significantly worse when the wake is detectable, between timestep 1200 and 1300. This coincides with one vessel occluding the other, and the combined effect of these two phenomena has a major negative effect on the extent estimate. This also affects the centroid estimate, resulting in a larger localization error. Utilizing negative information mitigates this effect since the occlusion is better managed and the effect of the wake clutter is somewhat mitigated by the extent estimate being corrected faster due to the use of negative information in

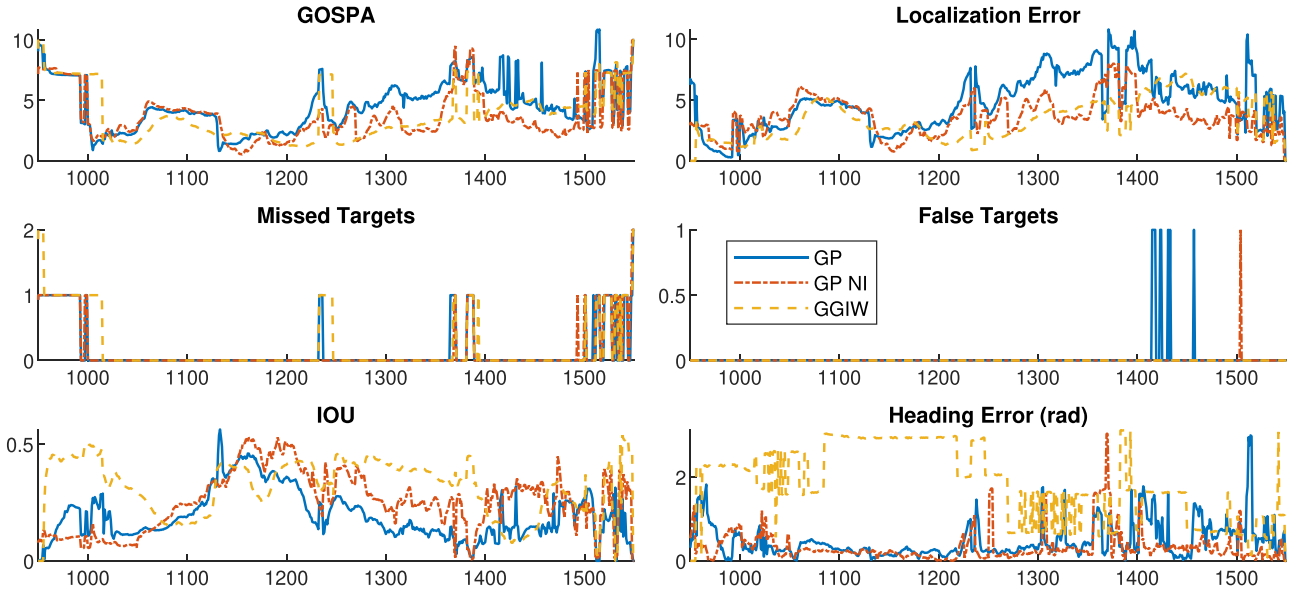

Figure 8. The evolution over the course of the multi-target test run for selected metrics.

the state estimate, but it is still worse than the GGIW model, albeit it is quicker to initialize an estimate, resulting in a lower share of missing targets and a lower GOSPA score. However, even with the use of negative information, the wake clutter still has an effect on the state estimate, as observed by the peak in localization error and the dip in IOU around 1230. The GGIW model is less affected by this shortcoming because of the assumption that measurements are uniformly distributed. Another thing of note is the relatively poor extent estimate of the GP methods at the beginning and the end of the scenario; this is due to scans from the LiDAR hitting at different heights of the target vessel, where the extent may be radically different. Since this method only utilizes information in 2D, this is a source of model inconsistency, and therefore the extent of the vessel is not estimated correctly. This is also a contributing factor to the GGIW model being able to estimate the extent better, which can be seen at the start of the scenario.

VII. CONCLUSION

This paper has presented the use of the GP model as a target model in the extended object PMBM-tracker, presented an improvement of the GP target model by using GN optimization, suggested a heuristic method to mitigate the fact that the measurement model is nonconvex, and we have highlighted the need for a well-designed birth density and provided an example. We have also presented a method to utilize negative information both to improve the state estimation and to handle occlusion. Furthermore, we have demonstrated the resulting tracker on both simulated and real data and compared the performance against the standard GGIW-PMBM tracker. It shows that the GP model can generally track targets more accurately, as measured by GOSPA, and provide a better extent estimate when only a part of the target is detected by the sensor, as measured by the IOU metric. It also enables a correct heading estimate since the heading is explicitly modeled as a part of the state. In addition, applying the method to real maritime data shows that wake clutter is an issue that needs to be addressed. The use of negative information further increases tracking performance and improves the state estimation. Furthermore, it specifically mitigates issues with occlusion and partially mitigates the effect of wake clutter, providing more robust performance on real maritime data.

A. Future Work

It would be of interest to look further into the issue of data association for this target model. Particularly given the computational cost of the method, of which the main part of the computational time is taken up by the data association step. Recent developments in this area for extended object PMBM filters have shown that it is possible to achieve a drastic reduction in computational time by reducing the PMBM to a PMB representation [7]. Directly estimating a PMB either by the use of belief propagation [8], [9] or blocked Gibbs sampling [30] has also shown a drastic reduction in computational time and better performance compared to estimating a PMBM. It would therefore be interesting to explore if the GP target model can be integrated into these methods. Another venue of future work would be to extend the method to also include 3D information, for which there already exist several target models [31], [32]. This would resolve the issue of model consistency when applying it to real data, which could prevent the issues where different LiDAR beams hit the target boat. It could also aid in reducing the effect of wake clutter on the extent estimate. It would also be of interest to directly incorporate a model that accounts for wake clutter into the filter. Recent work has explored how to model arbitrary sources of clutter in the PMBM framework [33], and wake clutter could be modeled in this framework. Clutter models for wake clutter in the context of target tracking already exist [34], [35], and they could be applied by adapting them to extended targets.

ACKNOWLEDGMENT

The authors would like to acknowledge the help of Øystein Kaarstad Helgesen in providing data sets from milliAmpere, Erik Wilthil at Zeabuz, and Egil Eide for assistance in collecting the data from milliAmpere2, and Simen Eldevik at DNV for providing ideas that contributed to the improvement of the Gauss–Newton optimization method used in the paper.

APPENDIX A

PARTIAL DERIVATIVES FOR NEGATIVE INFORMATION

Following the approach in [11], we divide the derivative into the following components:

$$\frac{dh^{max}(\mathbf{x})}{d\mathbf{x}} = \left[\frac{dh^{max}(\mathbf{x})}{d\mathbf{x}^c} \quad \frac{dh^{max}(\mathbf{x})}{d\phi} \quad \frac{dh^{max}(\mathbf{x})}{d\mathbf{x}^f} \right]. \tag{69}$$

The time index has been omitted for brevity. The derivatives can be found by applying the chain rule and the quotient rule. We start by making the substitution

$$u = \frac{u_y}{u_x} = \frac{y^p + \sin\left(\theta^f_{max} + \phi\right) \mathbf{H}^{\mathbf{f}} \left(\theta^f_{max}\right) \mathbf{x}^f}{x^p + \cos(\theta^f_{max} + \phi) \mathbf{H}^{\mathbf{f}} \left(\theta^f_{max}\right) \mathbf{x}^f}. \tag{70}$$

We also introduce the following shorthands:

$$\begin{aligned} \mathbf{H}^f\left(\theta^f_{max}\right) &= \mathbf{H}^f \\ \theta^f_{max} + \phi &= \theta^{(G)}_{max}. \end{aligned} \tag{71}$$

The derivative of $\arctan(u)$ is $\frac{1}{1+u^2}$; therefore, according to the chain rule, we get

$$\frac{dh^{max}(\mathbf{x})}{d\mathbf{x}} = \frac{1}{1+u^2} \left[\frac{du}{d\mathbf{x}^c} \quad \frac{du}{d\phi} \quad \frac{du}{d\mathbf{x}^f} \right]. \tag{72}$$

To calculate the partial derivatives, we apply the quotient rule. Doing this results in

$$\begin{aligned}
\frac{du}{dx^p} &= -\frac{y^p + \sin\left(\theta_{max}^{(G)}\right)\mathbf{H}^f\mathbf{x}^f}{{u_x}^2} \\
\frac{du}{dy^p} &= \frac{1}{u_x} \\
\frac{du}{d\phi} &= \frac{\mathbf{H}^f\mathbf{x}^f\left(\mathbf{H}^f\mathbf{x}^f + x^p\cos\left(\theta_{max}^{(G)}\right) + y^p\sin\left(\theta_{max}^{(G)}\right)\right)}{{u_x}^2} \\
\frac{du}{d\mathbf{x}^f} &= \frac{\mathbf{H}^f\left(x^p\sin\left(\theta_{max}^{(G)}\right) - y^p\cos\left(\theta_{max}^{(G)}\right)\right)}{{u_x}^2}.
\end{aligned} \tag{73}$$

By expanding

$$\frac{1}{1+u^2} = \frac{{u_x}^2}{{u_x}^2 + {u_y}^2}, \tag{74}$$

then multiplying this expression with the ones above we end up with the final partial derivatives

$$\begin{aligned}
\frac{du}{dx} &= -\frac{y + \sin\left(\theta_{max}^{(G)}\right)\mathbf{H}^f\mathbf{x}^f}{{u_x}^2 + {u_y}^2} \\
\frac{du}{dy} &= \frac{x^p + \cos\left(\theta_{max}^{(G)}\right)\mathbf{H}^f\mathbf{x}^f}{{u_x}^2 + {u_y}^2} \\
\frac{du}{d\phi} &= \frac{\mathbf{H}^f\mathbf{x}^f\left(\mathbf{H}^f\mathbf{x}^f + x\cos\left(\theta_{max}^{(G)}\right) + y\sin\left(\theta_{max}^{(G)}\right)\right)}{{u_x}^2 + {u_y}^2} \\
\frac{du}{d\mathbf{x}^f} &= \frac{\mathbf{H}^f\left(x\sin\left(\theta_{max}^{(G)}\right) - y\cos\left(\theta_{max}^{(G)}\right)\right)}{{u_x}^2 + {u_y}^2}.
\end{aligned} \tag{75}$$

It follows that the partial derivatives for the minimum angle can be found by substituting θ_{max}^f with θ_{min}^f.

APPENDIX B
PMBM FLTER RECURSIONS FOR A GP TARGET MODEL

B.1. Prediction

As stated in the main text, we utilize the expressions derived for an extended object PMBM filter in [3] and use those to derive closed-form expressions.

The posterior distribution of a PMBM prior is a PMBM with parameters

$$D_{k-1}^u, \{w_{k-1}^j, \{r_{k-1}^{j,i}, (f_{k-1}^{j,i})\}_{i\in\mathbb{I}_{k|k'}}\}_{j\in\mathbb{J}_{k|k'}}. \tag{76}$$

Then, the predicted distribution is a PMBM with parameters

$$D_{k|k-1}^u, \{w_{k|k-1}^j, \{r_{k|k-1}^{j,i}, (f_{k|k-1}^{j,i})\}_{i\in\mathbb{I}_{k|k'}}\}_{j\in\mathbb{J}_{k|k'}}, \tag{77}$$

where the parameters are given by

$$\begin{aligned}
D_{k|k-1}^u &= D^b(\mathbf{x}) + \langle D_{k-1}^u; P_S\mathbf{g}_{k|k-1}(\mathbf{x})\rangle \\
w_{k|k-1}^j &= w_{k-1}^j \\
r_{k|k-1}^{j,i} &= \langle f_{k-1}^{j,i}; P_S\rangle r_{k-1}^{j,i} \\
f_{k|k-1}^{j,i} &= \frac{\langle f_{k-1}^{j,i}; P_S\mathbf{g}_{k|k-1}(\mathbf{x})\rangle}{\langle f_{k-1}^{j,i}; P_S\rangle}.
\end{aligned} \tag{78}$$

For the Gaussians, we can derive the expressions using the product rule and integrating the resulting expression

$$\begin{aligned}
&\left\langle f_{k-1}^{j,i}; P_S\mathbf{g}_{k|k-1}(\mathbf{x})\right\rangle \\
&= P_S\int \mathcal{N}(\mathbf{x}_{k-1}; \mathbf{x}_{k-1}^{j,i}, \mathbf{P}_{k-1})\mathcal{N}(\mathbf{x}_k; \mathbf{F}\mathbf{x}', \mathbf{Q})d\mathbf{x}_{k-1} \\
&= P_S\mathcal{N}(\mathbf{x}_k; \mathbf{F}\mathbf{x}_{k-1}^{j,i}, \mathbf{F}\mathbf{P}_{k|k-1}^{j,1}\mathbf{F}^{\mathrm{T}} + \mathbf{Q})\int \mathcal{N}(\mathbf{x}_{k-1}; \cdot, \cdot)d\mathbf{x}_{k-1} \\
&= P_S\mathcal{N}(\mathbf{x}_k; \mathbf{F}\mathbf{x}_{k-1}^{j,i}, \mathbf{F}\mathbf{P}_{k|k-1}^{j,1}\mathbf{F}^{\mathrm{T}} + \mathbf{Q}) \\
&\langle D_{k-1}; P_S\mathbf{g}_{k|k-1}(\mathbf{x})\rangle \\
&= P_S\int \sum_{n=1}^{N^u} d_n^u\mathcal{N}(\mathbf{x}_{k-1}, \mathbf{x}_n^u, \mathbf{P}_n^u)\mathcal{N}(\mathbf{x}_k; \mathbf{F}\mathbf{x}', \mathbf{Q})d\mathbf{x}_{k-1} \\
&= P_S\sum_{n=1}^{N^u} d_n^u\mathcal{N}(\mathbf{x}_k; \mathbf{F}\mathbf{x}_n^u, \mathbf{F}\mathbf{P}_n^u\mathbf{F}^{\mathrm{T}} + \mathbf{Q})\int \mathcal{N}(\mathbf{x}_{k-1}; \cdot, \cdot)d\mathbf{x}_{k-1} \\
&= P_S\sum_{n=1}^{N^u} d_n^u\mathcal{N}(\mathbf{x}_k; \mathbf{F}\mathbf{x}_n^u, \mathbf{F}\mathbf{P}_n^u\mathbf{F}^{\mathrm{T}} + \mathbf{Q}) \\
&\left\langle f_k^{j,i}; P_S\right\rangle = P_S\int f_{k-1}^{j,i}(\mathbf{x})d\mathbf{x} = P_S.
\end{aligned} \tag{79}$$

The gamma component does not have a similar expression, and we instead use the heuristic defined in [24] and presented in (18). Inserting these expressions into (78) and simplifying results in (34).

B.2. Update

Starting with the predicted PMBM and given the set of measurements Z_k. The posterior distribution is then also a PMBM with parameters

$$D_k^u, \{w_k^{j,A}, \{r_k^{j,C}, (f_k^{j,C})\}_{C\in A}\}_{j\in\mathbb{J}_{k|k-1}, A\in\mathcal{A}^j}, \tag{80}$$

where $\mathcal{A}^j$ is the set of all possible data associations for the association hypothesis with index j. If measurement cell C belongs to a detected target, the following

expressions apply:

$$
\begin{aligned}
L_C^j &= \begin{cases} 1 - r_{k|k-1}^{j,i_C} + r_{k|k-1}^{j,i_C} \langle f_{k|k-1}^{j,i_C}; Q_D \rangle & |Z_C| = 0 \\ r_{k|k-1}^{j,i_C} \langle f_{k|k-1}^{j,i_C}; l(Z_C|\mathbf{x}) \rangle & |Z_C| \neq 0 \end{cases} \\
r_k^{j,i_C} &= \begin{cases} \frac{r_{k|k-1}^{j,i_C} \langle f_{k|k-1}^{j,i_C}; Q_D \rangle}{1 - r_{k|k-1}^{j,i_C} + r_{k|k-1}^{j,i_C} \langle f_{k|k-1}^{j,i_C}; Q_D \rangle} & |Z_C| = 0 \\ 1 & |Z_C| \neq 0 \end{cases} \\
f_k^{j,i_C}(\mathbf{x}) &= \begin{cases} \frac{Q_D f_{k|k-1}^{j,i_C}}{\langle Q_D; f_{k|k-1}^{j,i_C} \rangle} & |Z_C| = 0 \\ \frac{l(Z_C|\mathbf{x}) f_{k|k-1}^{j,i_C}}{\langle l(Z_C|\mathbf{x}); f_{k|k-1}^{j,i_C} \rangle} & |Z_C| \neq 0 \end{cases}.
\end{aligned} \tag{81}
$$

If measurements are assigned to an undetected target, we instead have the following expressions:

$$
\begin{aligned}
L_C^j &= \begin{cases} D^c + \langle D_{k|k-1}^u; l(Z_C|\mathbf{x}) \rangle & |Z_C| = 1 \\ \langle D_{k|k-1}^u; l(Z_C|\mathbf{x}) \rangle & |Z_C| > 1 \end{cases} \\
r_k^{j,i_C} &= \begin{cases} \frac{\langle D_{k|k-1}^u; l(Z_C|\mathbf{x}) \rangle}{D^c + \langle D_{k|k-1}^u; l(Z_C|\mathbf{x}) \rangle} & |Z_C| = 1 \\ 1 & |Z_C| > 1 \end{cases} \\
f_k^{j,i_C}(\mathbf{x}) &= \frac{l(Z_C|\mathbf{x}) D_{k|k-1}^u}{\langle l(Z_C|\mathbf{x}); D_{k|k-1}^u \rangle}.
\end{aligned} \tag{82}
$$

Q_D is assumed scalar, so we get

$$
\begin{aligned}
\langle Q_D; f_{k|k-1}^{j,i_C} \rangle &= Q_D \int f_{k|k-1}^{j,i_C}(\mathbf{x}) d\mathbf{x} = Q_D \\
\langle Q_D; D_{k|k-1}^u \rangle &= Q_D \int D_{k|k-1}^u(\mathbf{x}) d\mathbf{x} = Q_D \\
Q_D f_{k|k-1}^{j,i_C} &= Q_D \mathcal{N}(\mathbf{x}, \mathbf{x}_{k|k-1}^{j,i}, \mathbf{P}_{k|k-1}),
\end{aligned} \tag{83}
$$

where the integrals all evaluate to 1 since the integrands are probability distribution functions. The remaining expressions are a collection of products and inner products of distributions. We can write a generic product

$$
\begin{aligned}
&p(\mathbf{x}) l(Z_C|\mathbf{x}) = \\
&P_D \mathcal{N}(\mathbf{x}; \hat{\mathbf{x}}_{k|k-1}, \mathbf{P}_{k|k-1}) \mathcal{G}(\lambda_m; \alpha_{k|k-1}, \beta_{k|k-1}) \\
&\quad \times P_D e^{-\lambda_m} \lambda_m^{|Z_C|} \mathcal{N}(\mathbf{z}; \mathbf{H}\mathbf{x}, \mathbf{R}).
\end{aligned} \tag{84}
$$

Given that we have assumed independence between the measurement rate and the combined state and extent, we can treat the Gaussian components and the gamma and Poisson components separately. First, we evaluate the products of the Gaussian distributions, which is done using the product rule for Gaussians, which states that

$$
\begin{aligned}
&\mathcal{N}(\mathbf{z}; \mathbf{H}\mathbf{x}, \mathbf{R}) \mathcal{N}(\mathbf{x}; \hat{\mathbf{x}}_{k|k-1}, \mathbf{P}_{k|k-1}) \\
&= \mathcal{N}(\mathbf{z}; \mathbf{H}\hat{\mathbf{x}}_{k|k-1}, \mathbf{S}) \mathcal{N}(\mathbf{x}; \hat{\mathbf{x}}_k, \mathbf{P}_k),
\end{aligned} \tag{85}
$$

where the first term is recognized as the posterior distribution and the second term is the predictive likelihood. The inner product can consequently be written as

$$
\begin{aligned}
&\int \mathcal{N}(\mathbf{z}; \mathbf{H}\mathbf{x}, \mathbf{R}) \mathcal{N}(\mathbf{x}; \mathbf{x}_{k|k-1}, \mathbf{P}_{k|k-1}) d\mathbf{x} \\
&= \mathcal{N}(\mathbf{z}; \mathbf{H}\hat{\mathbf{x}}_{k|k-1}, \mathbf{S}) \int \mathcal{N}(\mathbf{x}; \hat{\mathbf{x}}_k, \mathbf{P}_k) d\mathbf{x} \\
&= \mathcal{N}(\mathbf{z}; \mathbf{H}\hat{\mathbf{x}}_{k|k-1}, \mathbf{S}),
\end{aligned} \tag{86}
$$

which corresponds to a marginalization of $\mathbf{x}$. For the gamma component, the key element is that the gamma distribution is the conjugate prior of the Poisson distribution, and the number of measurements $|Z_C|$ is Poisson distributed $\mathcal{PS}(|Z_C|; \lambda_m)$. In [24], it was shown that the product evaluates to

$$
\begin{aligned}
&\mathcal{G}(\lambda_m; \alpha_{k|k-1}, \beta_{k|k-1}) \mathcal{PS}(|Z_C|; \lambda_m) \\
&= \mathcal{G}(\lambda_m; \alpha_{k|k-1} + |Z_C|, \beta_{k|k-1} + 1) \\
&\quad \times \frac{\Gamma(\alpha_{k|k-1} + |Z_C|) \beta_{k|k-1}^{\alpha_{k|k-1}}}{\Gamma(\alpha_{k|k-1}) (\beta_{k|k-1} + 1)^{(\alpha_{k|k-1} + |Z_C|)} |Z_C|!},
\end{aligned} \tag{87}
$$

where the first term is the posterior of the gamma distribution and the second term is the predictive likelihood. From this, we can combine the two expressions and write a combined predictive likelihood as

$$
\begin{aligned}
l_C(\alpha, \beta, \mathbf{x}, \mathbf{P}, Z_C) = P_D &\frac{\Gamma(\alpha + |Z_C|) \beta^\alpha}{\Gamma(\alpha) (\beta + 1)^{(\alpha + |Z_C|)} |Z_C|!} \\
&\times \mathcal{N}(\mathbf{z}; \mathbf{H}\hat{\mathbf{x}}_{k|k-1}, \mathbf{S}).
\end{aligned} \tag{88}
$$

The posterior can be found from Bayes rule

$$
\frac{p(\mathbf{x}) l(Z_C|\mathbf{x})}{\langle p(\mathbf{x}); l(Z_C|\mathbf{x}) \rangle} = \mathcal{N}(\mathbf{x}; \hat{\mathbf{x}}_k, \mathbf{P}_k) \mathcal{G}(\lambda_m; \alpha_k, \beta_k). \tag{89}
$$

Replacing the generic probability density p with f^{j,i_C} or the components of the mixture D^u results in the following predictive likelihoods:

$$
\begin{aligned}
\langle l(Z_C|\mathbf{x}); f_{k|k-1}^{j,i_C} \rangle &= l_C(\alpha^{j,i_C}, \beta^{j,i_C}, \mathbf{x}_{k|k-1}^{j,i_C}, \mathbf{P}_{k|k-1}^{j,i_C}, Z_C) \\
\langle l(Z_C|\mathbf{x}); D_{k|k-1}^u \rangle &= \sum_{n=1}^{N^u} d_n^u l_C(\alpha_n^u, \beta_n^u, \mathbf{x}_n^u, \mathbf{P}_n^u, Z_C)
\end{aligned} \tag{90}
$$

and the following posterior distributions:

$$
\begin{aligned}
\frac{l(Z_C|\mathbf{x}) D_{k|k-1}^u}{\langle l(Z_C|\mathbf{x}); D_{k|k-1}^u \rangle} &= \sum_{n=1}^{N^u} d_n^u \mathcal{N}(\mathbf{x}; \hat{\mathbf{x}}_n^u, \hat{\mathbf{P}}_n^u) \mathcal{G}(\alpha_n^u, \beta_n^u) \\
\frac{l(Z_C|\mathbf{x}) f_{k|k-1}^{j,i_C}}{\langle l(Z_C|\mathbf{x}); f_{k|k-1}^{j,i_C} \rangle} &= \mathcal{N}(\mathbf{x}; \hat{\mathbf{x}}_k^{j,i_C}, \hat{\mathbf{P}}_k^{j,i_C}) \mathcal{G}(\alpha_k^{j,i_C}, \beta_k^{j,i_C}).
\end{aligned} \tag{91}
$$

Inserting these expressions into (81) and (82) results in (46) and (47), respectively.

REFERENCES

[1] K. Granström, M. Baum, and S. Reuter
"Extended object tracking: Introduction, overview and applications,"
J. Adv. Inf. Fusion, vol. 12, no. 2, pp. 139–174, Dec. 2017.

[2] J. W. Koch
"Bayesian approach to extended object and cluster tracking using random matrices,"
IEEE Trans. Aerosp. Electron. Syst., vol. 44, no. 3, pp. 1042–1059, Jul. 2008.

[3] K. Granström, M. Fatemi, and L. Svensson
"Poisson multi-Bernoulli mixture conjugate prior for multiple extended target filtering,"
IEEE Trans. Aerosp. Electron. Syst., vol. 56, no. 1, pp. 208–225, Feb. 2020.

[4] J. L. Williams
"Marginal multi-Bernoulli filters: RFS derivation of MHT, JIPDA, and association-based member,"
IEEE Trans. Aerosp. Electron. Syst., vol. 51, no. 3, pp. 1664–1687, Jul. 2015.

[5] Y. Xia, K. Granström, L. Svensson, A. F. García-Fernández, and J. L. Williams
"Extended target Poisson multi-Bernoulli mixture trackers based on sets of trajectories,"
in *Proc. 22th Int. Conf. Inf. Fusion*, Jul. 2019, pp. 1–8.

[6] K. Granström, L. Svensson, S. Reuter, Y. Xia, and M. Fatemi
"Likelihood-based data association for extended object tracking using sampling methods,"
IEEE Trans. Intell. Veh., vol. 3, no. 1, pp. 30–45, Mar. 2018.

[7] Y. Xia, K. Granström, L. Svensson, M. Fatemi, A. F. García-Fernández, and J. L. Williams
"Poisson multi-Bernoulli approximations for multiple extended object filtering,"
IEEE Trans. Aerosp. Electron. Syst., vol. 58, no. 2, pp. 890–906, Apr. 2022.

[8] Y. Xia, A. F. García-Fernández, F. Meyer, J. L. Williams, K. Granström, and L. Svensson
"Trajectory PMB filters for extended object tracking using belief propagation,"
IEEE Trans. Aerosp. Electron. Syst., vol. 59, no. 6, pp. 9312–9331, 2023.

[9] F. Meyer and J. L. Williams
"Scalable detection and tracking of geometric extended objects,"
IEEE Trans. Signal Process., vol. 69, pp. 6283–6298, 2021.

[10] M. Baum and U. D. Hanebeck
"Shape tracking of extended objects and group targets with star-convex RHMs,"
in *Proc. 14th Int. Conf. Inf. Fusion*, 2011, pp. 1–8.

[11] N. Wahlstrom and E. Ozkan
"Extended target tracking using Gaussian processes,"
IEEE Trans. Signal Process., vol. 63, no. 16, pp. 4165–4178, Aug. 2015.

[12] M. Kumru, H. Köksal, and E. Özkan
"Variational measurement update for extended object tracking using Gaussian processes,"
IEEE Signal Process. Lett., vol. 28, pp. 538–542, 2021.

[13] M. Michaelis, P. Berthold, T. Luettel, D. Meissner, and H.-J Wuensche
"Extended object tracking with an improved measurement-to-contour association,"
in *Proc. IEEE 23rd Int. Conf. Inf. Fusion*, Jul. 2020, pp. 1–6.

[14] S. Lee and J. McBride
"Extended object tracking via positive and negative information fusion,"
IEEE Trans. Signal Process., vol. 67, no. 7, pp. 1812–1823, Apr. 2019.

[15] T. Hirscher, A. Scheel, S. Reuter, and K. Dietmayer
"Multiple extended object tracking using Gaussian processes,"
in *Proc. 19th Int. Conf. Inf. Fusion*, 2016, pp. 868–875.

[16] M. Michaelis, P. Berthold, D. Meissner, and H.-J Wuensche
"Heterogeneous multi-sensor fusion for extended objects in automotive scenarios using Gaussian processes and a GMPHD-filter,"
in *Proc. Sensor Data Fusion: Trends, Solutions, Appl. (SDF)*, 2017, pp. 1–6.

[17] Y. Xia, K. Granström, L. Svensson, and A. F. García-Fernández
"Performance evaluation of multi-Bernoulli conjugate priors for multi-target filtering,"
in *Proc. 20th Int. Conf. Inf. Fusion*, 2017, pp. 1–8.

[18] K. Granström, C. Lundquist, and O. Orguner
"Extended target tracking using a Gaussian-mixture PHD filter,"
IEEE Trans. Aerosp. Electron. Syst., vol. 48, no. 4, pp. 3268–3286, Oct. 2012.

[19] K. Granström and U. Orguner
"A PHD filter for tracking multiple extended targets using random matrices,"
IEEE Trans. Signal Process., vol. 60, no. 11, pp. 5657–5671, Nov. 2012.

[20] K. Wyffels and M. Campbell
"Negative information for occlusion reasoning in dynamic extended multiobject tracking,"
IEEE Trans. Robot., vol. 31, no. 2, pp. 425–442, Apr. 2015.

[21] M. Baerveldt, M. E. Lopez, and E. F. Brekke
"Extended target PMBM tracker with a Gaussian process target model on LiDAR data,"
in *Proc. 26th Int. Conf. Inf. Fusion*, 2023, pp. 8.

[22] C. E. Rasmussen and C. K. I. Williams
Gaussian Processes for Machine Learning, in Adaptive Computation and Machine Learning. Cambridge, MA, USA: MIT Press, 2006.

[23] M. E. Lopez
"Poisson multi-Bernoulli mixture filter for multiple extended object tracking of maritime vessels using LiDAR and Gaussian processes," 2020. [Online]. Available: https://ntnuopen.ntnu.no/ntnu-xmlui/handle/11250/2781005

[24] K. Granström and U. Orguner
"Estimation and maintenance of measurement rates for multiple extended target tracking,"
in *Proc. 15th Int. Conf. Inf. Fusion*, 2012, pp. 2170–2176.

[25] C. Lundquist, K. Granström, and U. Orguner
"An extended target CPHD filter and a gamma Gaussian inverse Wishart implementation,"
IEEE J. Sel. Topics Signal Process., vol. 7, no. 3, pp. 472–483, Jun. 2013.

[26] B. Bell and F. Cathey
"The iterated Kalman filter update as a Gauss–Newton method,"
IEEE Trans. Autom. Control, vol. 38, no. 2, pp. 294–297, Feb. 1993.

[27] A. S. Rahmathullah, A. F. García-Fernández, and L. Svensson
"Generalized optimal sub-pattern assignment metric,"
in *Proc. 20th Int. Conf. Inf. Fusion*, 2017, pp. 1–8.

[28] E. F. Brekke, E. Eide, B.-O. H. Eriksen, E. F. Wilthil, M. Breivik, E. Skjellaug, Ø. K. Helgesen, A. M. Lekkas, A. B. Martinsen, E. H. Thyri, T. Torben, E. Veitch, O. A. Alsos, and T. A. Johansen
"milliAmpere: An Autonomous Ferry Prototype," J. Phys.: Conf. Ser., vol. 2311, no. 1, pp. 012029, Jul. 2022, publisher: IOP Publishing.

[29] Ø. K. Helgesen, K. Vasstein, E. F. Brekke, and A. Stahl
"Heterogeneous multi-sensor tracking for an autonomous surface vehicle in a littoral environment,"
Ocean Eng., vol. 252, May 2022.

[30] Y. Xia, A. F. García-Fernández, and L. Svensson
"An efficient implementation of the extended object trajectory PMB filter using blocked Gibbs sampling,"
in *Proc. 26th Int. Conf. Inf. Fusion*, 2023, pp. 1–8.

[31] M. Kumru and E. Özkan
"Three-dimensional extended object tracking and shape learning using Gaussian processes,"

IEEE Trans. Aerosp. Electron. Syst., vol. 57, no. 5, pp. 2795–2814, Oct. 2021.

[32] T. Baur, J. Reuter, A. Zea, and U. D. Hanebeck "Extent estimation of sailing boats applying elliptic cones to 3D LiDAR data," in *Proc. 2022 25th Int. Conf. Inf. Fusion*, 2022, pp. 1–8.

[33] A. F. García-Fernández, Y. Xia, and L. Svensson "Poisson multi-Bernoulli mixture filter with general target-generated measurements and arbitrary clutter," *IEEE Trans. Signal Process.*, vol. 71, pp. 1895–1906, 2023.

[34] E. Brekke, O. Hallingstad, and J. Glattetre "Improved target tracking in the presence of wakes," *IEEE Trans. Aerosp. Electron. Syst.*, vol. 48, no. 2, pp. 1005–1017, 2012.

[35] A. G. Hem, H.-G. Alvheim, and E. F. Brekke "Wakeipda: Target tracking with existence modeling in the presence of wakes," in *Proc. 26th Int. Conf. Inf. Fusion*, 2023, pp. 1–7.

Martin Baerveldt received the M.Sc. degree in complex adaptive systems from Chalmers University of Technology, Gothenburg, Sweden, in 2019. He is currently pursuing Ph.D. at the Department of Engineering Cybernetics, Norwegian University of Science and Technology (NTNU), Trondheim, Norway. He is a part of the European training and research network on Autonomous Barges for Smart Inland Shipping (AUTOBarge). His research focuses on automated situational awareness with a view to autonomous surface vessels, with a particular focus on extended object tracking.

Michael Ernesto López received the M.Sc. degree in mathematics from the Complutense University of Madrid, Spain, in 2012, and the M.Sc. degree in engineering cybernetics from Norwegian University of Science and Technology (NTNU), Trondheim, Norway, in 2021. Since 2021, he has been pursuing Ph.D. at the Department of Engineering Cybernetics, NTNU, with a focus on detection and pose estimation of maritime vessels.

Edmund Førland Brekke received the M.Sc. degree in industrial mathematics in 2005 and the Ph.D. degree in engineering cybernetics in 2010, both from the Norwegian University of Science and Technology (NTNU), Trondheim, Norway. From 2010 to 2014, he worked with the Acoustic Research Laboratory (ARL), NUS in Singapore as a Postdoctoral Research Fellow. In 2014, he rejoined NTNU and the Department of Engineering Cybernetics, where he is currently a Professor of sensor fusion. Brekke's research interests are in the area of sensor fusion and situational awareness, with a particular focus on multitarget tracking and maritime surface autonomy. He is an Associate Editor of the IEEE Journal of Oceanic Engineering.